

The Fragile Nature of Road Transportation Systems

Linghang Sun^{a,*}, Yifan Zhang^a, Cristian Axenie^b, Margherita Grossi^c, Anastasios Kouvelas^a,
Michail A. Makridis^a

^a*Institute for Transport Planning and Systems, ETH Zurich, Zurich, 8093, Switzerland*

^b*Computer Science Department and Center for Artificial Intelligence, Technische Hochschule
Nürnberg, Nürnberg, 90489, Germany*

^c*Intelligent Cloud Technologies Lab, Huawei Munich Research Center, Munich, 80992, Germany*

Abstract

Major cities worldwide experience problems with the performance of their road transportation systems, and the continuous increase in traffic demand presents a substantial challenge to the optimal operation of urban road networks and the efficiency of traffic control strategies. The operation of transportation systems is widely considered to display fragile property, i.e., the loss in performance increases exponentially with the linearly increasing magnitude of disruptions. Meanwhile, the risk engineering community is embracing the novel concept of antifragility, enabling systems to learn from historical disruptions and exhibit improved performance under black swan events. In this study, based on established traffic models, namely fundamental diagrams and macroscopic fundamental diagrams, we first conducted a rigorous mathematical analysis to prove the fragile nature of road transportation systems theoretically. Subsequently, we propose a skewness-based indicator that can be readily applied to cross-compare the degree of fragility for different networks solely dependent on the MFD-related parameters. At last, by taking real-world stochasticity into account, we implemented a numerical simulation with realistic network data to bridge the gap between the theoretical proof and the real-world operations, to reflect the potential impact of uncertainty on the fragility of the systems. This work aims to demonstrate the fragile nature of road transportation systems and help researchers better comprehend the necessity to consider explicitly antifragile design for future traffic control strategies.

Keywords: antifragility, traffic disruptions, road transportation systems, macroscopic fundamental diagram, fragility indicator

1. Introduction

As reported by both the [U.S. Department of Transportation \(2019\)](#) and the [Federal Statistical Office of Switzerland \(2020\)](#), motorized road traffic before the pandemic has experienced an approximate 50% growth over the past few decades. Researchers have also found that the continuous growth in traffic volume has consequently contributed to a rise in disruptive events, such as severe congestion and more frequent accidents ([Dickerson et al., 2000](#)). With evidence confirming the recovery of individual motorized traffic from the pandemic ([Büchel et al., 2022](#); [Marra et al., 2022](#)), it is expected that this upward trend will continue in the coming decades, even with the political and behavioral shift being taken into account, such as bicycle-friendly design

*Corresponding author.

Email address: lisun@ethz.ch (Linghang Sun)

and working-from-home (Zhang and Zhang, 2021). Matthias et al. (2020) shows that although Germany is widely regarded as an active player in carbon neutrality, motorized traffic is still projected to increase following a more politically regulated sustainable development. Another emerging transformation often disregarded is the deployment of Autonomous Vehicles (AVs) and autonomous mobility-on-demand, which may account for more than 10% growth in terms of induced demand (Nahmias-Biran et al., 2021). Therefore, future road networks are highly expected to experience a further increase in traffic demand.

Meanwhile, there is a common understanding that road transportation networks can exhibit fragile properties. Fragility signifies a system’s susceptibility to exponentially escalating performance deterioration as disruptions increase in magnitude. One prominent and intuitive example of such fragile characteristics is the BPR function (U.S. Bureau of Public Roads, 1964), which distinctly illustrates with empirical data at the link level that travel time grows exponentially with traffic flow, leading to an infinite temporal cost when the traffic influx is at the maximal density of the network. Moreover, not limited to urban road networks, many other types of transportation systems can also display similar fragile responses to increasing disruption levels, such as in railway (Saidi et al., 2023) and aviation systems (U.S. Congress, Office of Technology Assessment, 1984).

Researchers have devoted extensive efforts to the assessment and design of robust and resilient transportation systems of all kinds, such as in railway systems (Corman et al., 2014), public transportation operation (Cats, 2016), aviation (Isaacson et al., 2010), and road networks (Ampountolas et al., 2017; Yang et al., 2019; Leclercq et al., 2021). However, when accounting for the ever-growing traffic volume in urban road networks and the exponentially escalating adversarial consequences, it is natural for us to wonder whether the current level of robustness and resilience can still guarantee the performance of road networks considering a long-term time horizon. Hence, we introduce the cutting-edge concept of antifragility to explain the phenomenon that urban road performance deteriorates exponentially with linearly growing disruptions. Previous studies on traffic performance showing signs of fragility, such as the BPR function, have primarily relied on empirical data and intuitive reasoning rather than rigorous mathematical proof. This paper, on the other hand, makes the following contributions:

1. *Proof of concept:* This research aims to establish the fragile nature of road transportation systems with a framework through mathematical analysis considering different aspects, that are at the link and the network levels, under demand and supply disruption, as well as considering the onset of disruption and recovery from disruption.
2. *Methodological contribution:* A skewness-based fragility indicator inspired by the Sigmoid curve is developed for the approximation of the fragility of a specific network. A scalable unit MFD can be applied for the cross-comparison of the fragility among different networks, relying on merely the parameters with physical meanings.
3. *From theory to reality:* As stochasticity prevails in road transportation systems in the real world, we also designed a numerical simulation considering real-world stochasticity, to study to what extent such realistic uncertainties can influence the fragile characteristics of transportation systems.

The overarching objective of this paper is to provide insights to transportation researchers for the future design of transportation systems and control strategies to be not only robust and resilient but also antifragile.

The remainder of this paper is structured as follows. Section 2 introduces antifragility and reviews specific traffic-related mathematical models. Section 3 formulates the mathematical definition of (anti-)fragility and its detection methods. Then we conduct the mathematical proof to establish such fragile nature in Section 4, whereas a skewness-based fragility indicator is proposed in Section 5. Section 6 presents the numerical simulation with real-world network and stochasticity. With Section 7, we conclude the fragile nature of road transportation systems and its implications for future studies.

2. Relevant Literature

Various terminologies have been proposed to evaluate the performance of road transportation systems, including their control strategies, and two commonly used terms to characterize the extent of performance variations under stress are robustness (Shang et al., 2022) and resilience (Mattsson and Jenelius, 2015; Calvert and Snelder, 2018). However, the definitions of robustness and resilience can vary under different contexts, even within the transportation domain itself, and are sometimes used interchangeably due to the different backgrounds and points of view of the authors (Corman et al., 2018; Tang et al., 2020). In this study, we adopt the definition proposed in Zhou et al. (2019), wherein robustness involves evaluating a system’s ability to maintain its initial state and withstand performance degradation when confronted with uncertainties and disturbances. On the other side, resilience emphasizes a system’s capability and promptness to recover from major disruptions and return to its original state. In brief, robustness relates to resistance, whereas resilience is about recovery. Another very recent term attracting much attention is the self-organized criticality of traffic flow from a complex systems perspective (Laval, 2023), implying an avalanche effect of unforeseeable magnitude when traffic ever becomes critical, which resembles the philosophy of optimality versus fragility.

Nevertheless, both robustness and resilience can overlook the consideration of a longer timespan, which is particularly relevant in transportation as the traffic demand grows continuously and consequently so as the occurrences of accidents. Thus, it is necessary to introduce a new term to address this gap. The novel concept of antifragility was initially proposed in Taleb (2012) and mathematically elaborated in Taleb and Douady (2013), and it serves as a general concept aimed at transforming people’s understanding and perception of risk. By embracing current risks, we can potentially leverage and adapt to future risks of greater magnitudes. When employed in systems and control, (anti-)fragility can be conceptualized as a nonlinear relationship between the performance and the magnitude of disruptions. If the performance is compromised due to unexpected disruptions, the relationship between the loss in performance and the disruptions would be convex for a fragile system, while being concave for an antifragile system. Ever since being proposed, antifragility has gained popularity in the risk engineering community and across multiple disciplines, such as biology (Kim et al., 2020), medicine (Axenie et al., 2022), energy (Coppitters and Contino, 2023), robotics (Axenie and Saveriano, 2023), and lately in transportation (Sun et al., 2024). It should also be highlighted that although systems can be fragile by nature, proper intervention and control strategies can enhance their antifragility against increasing levels of disruptions (Axenie et al., 2024).

For each link in a highway network, the BPR function (U.S. Bureau of Public Roads, 1964), as shown in Eq. 1, has given an intuitive example showing the fragility of the transportation systems at a link level. As the traffic flow q approaches the capacity of a link q_{\max} , the travel time T is revealed to grow exponentially compared to the free flow travel time T_{ff} . The BPR

function and its variations have been extensively applied in the estimation of the link (route) travel time (Lo et al., 2006; Ng and Waller, 2010; Wang et al., 2014). However, to uphold the statement that road transportation systems are fragile in general, an empirical function like BPR alone is not sufficient without rigid mathematical proof. It is also desired to show the fragility more broadly, i.e., not only at the link level but also at the network level, as well as for different types of disruptions.

$$T = T_{ff} \left(1 + 0.15 \left(\frac{q}{q_{\max}} \right)^4 \right) \quad (1)$$

The assessment of the traffic performance of road transportation systems can be conducted at either the link or the network level. However, due to the non-identical traffic characteristics across different levels, researchers have formulated diverse models to offer a more precise description of traffic dynamics at these levels, demonstrating the mathematical relationship between traffic flow, denoted as q , traffic density, denoted as k , and sometimes also traffic speed, denoted as $v = \frac{q}{k}$. While some traffic models are generated numerically from data collected with sensors such as loop detectors or aerial photos, others are derived through analytical methods (Mariotte et al., 2017). Typically, these models also involve a critical density, denoted as k_c , below which the flow increases as density rises, but beyond which the flow decreases as density continues to increase until reaching the maximal density, denoted as k_{\max} .

The earliest study on traffic performance was carried out and described in Greenshields et al. (1934) at a section of a highway and yielded the first Fundamental Diagram (FD), as shown in Fig. 1(a) exhibiting the relationship between traffic flow and density at the link level in the shape of a second-degree polynomial. Later, other researchers also developed FDs in various forms, with one of the most commonly applied FDs being proposed in Daganzo (1994), as shown in Fig. 1(b), which is characterized by two linear functions. While the Greenshields FD is entirely generated by fitting the polynomial coefficients with on-site data, the Daganzo FD, on the other hand, is derived analytically by treating the traffic flow hydrodynamically and incorporates variables with physical meanings, namely the gradient of the line segment below k_c as the free-flow speed, represented by u_f , and the gradient of the line segment beyond k_c as the backward wave speed, represented by w , a virtual wave of reduced speed and increased density propagating against the direction of traffic flow when vehicles are forced to stop.

On the network level, with the assumption of a homogeneous region, a Macroscopic Fundamental Diagram (MFD) can be produced by aggregating data points gathered from representative links within a network. Similar to FDs, MFDs can be approximated through different models, and the most widely applied functional forms include polynomials and multi-regime linear functions. MFDs can be fit numerically from field measurements as a cubic polynomial, as in Haddad and Shraiber (2014); Sirmatel and Geroliminis (2018) and illustrated in Fig. 2(a). Therefore, it's commonly seen in research works simulating traffic control at a network level with a given MFD. On the other hand, based on variation theory (Daganzo, 2005) and the assumption to simply a homogenous network into an abstract corridor, Daganzo and Geroliminis (2008) is the first study to generate an MFD analytically, and is often referred to as the Method of Cuts (MoC). Instead of installing loop detectors under the pavement and gathering massive traffic flow data, MoC can be applied to derive an MFD directly from traffic-related variables with physical meanings, such as free flow speed, traffic signal cycle, lane length, etc. An example of multi-regime linear functions MFD from MoC is shown in Fig. 2(b). Although theoretically

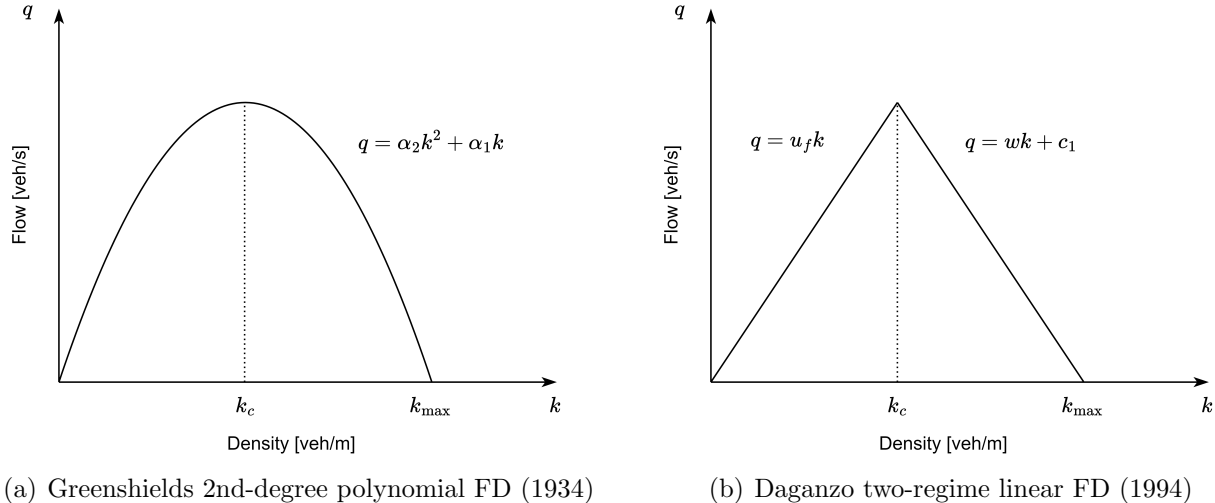


Figure 1: Mathematical models of FDs

an infinite number of cuts can be generated to approximate the MFD, only the practical cuts, the solid lines as shown in Fig. 2(b), are used for simplicity. [Leclercq and Geroliminis \(2013\)](#) improved the original MoC to accommodate topology and signal timing heterogeneity within the network. [Ambühl et al. \(2019\)](#); [Saedi et al. \(2020\)](#) also introduced algorithms to partition an entire heterogeneous network into multiple more homogeneous regions. The most recent advance in the study of MFD built on MoC is [Tilg et al. \(2023\)](#), which relaxes the assumption of demand homogeneity and an abstract corridor by creating a hypernetwork from a set of corridors and incorporating turn ratios between corridors. Although some other analytical methods have also been proposed to produce an MFD, such as through stochastic approximation ([Laval and Castrión, 2015](#)), [Tilg et al. \(2020\)](#) has demonstrated that MoC yields a more accurate upper bound for the MFD. Lately, researchers have also explored the potential utilization of MFD in railway ([Corman et al., 2019](#)) and aviation operations ([Safadi et al., 2023](#)), which yields some positive possibilities of extending the MFD into other modes.

As also acknowledged in these works, some variables, particularly the parameters related to signalization, can be hard to acquire in the real world with actuated signals. Therefore, simplified MFDs are also widely adopted when solving more applicational problems in the real world. [Daganzo et al. \(2018\)](#) approximated a simplified MoC-based MFD using only three cuts from one of each stationary, forward, and backward observer, and formed the trapezoidal uMFD. Moreover, one shortcoming of the numerical-based MFD is that, since the data points near the maximal density k_{\max} are scarce overall, the approximated MFD can lose its fidelity near k_{\max} . For example, the third-degree polynomial in [Geroliminis et al. \(2013\)](#) has only one real root, indicating the speed is above zero despite the network already reaching a gridlock, which is unrealistic. As claimed in [Daganzo and Geroliminis \(2008\)](#), since MFDs should be concave, the flow and speed are both zero by definition at maximal density.

The above discussion in the literature is confined to the flow-density MFD. However, assuming the total lane length and average trip length, denoted by D and L respectively, are known for a given network, the trip completion (sometimes also referred to as network production or outflow rate in different research works) denoted by m , and vehicle accumulation within the network denoted by n , can be further determined ([Leclercq and Geroliminis, 2013](#); [Geroliminis et al.,](#)

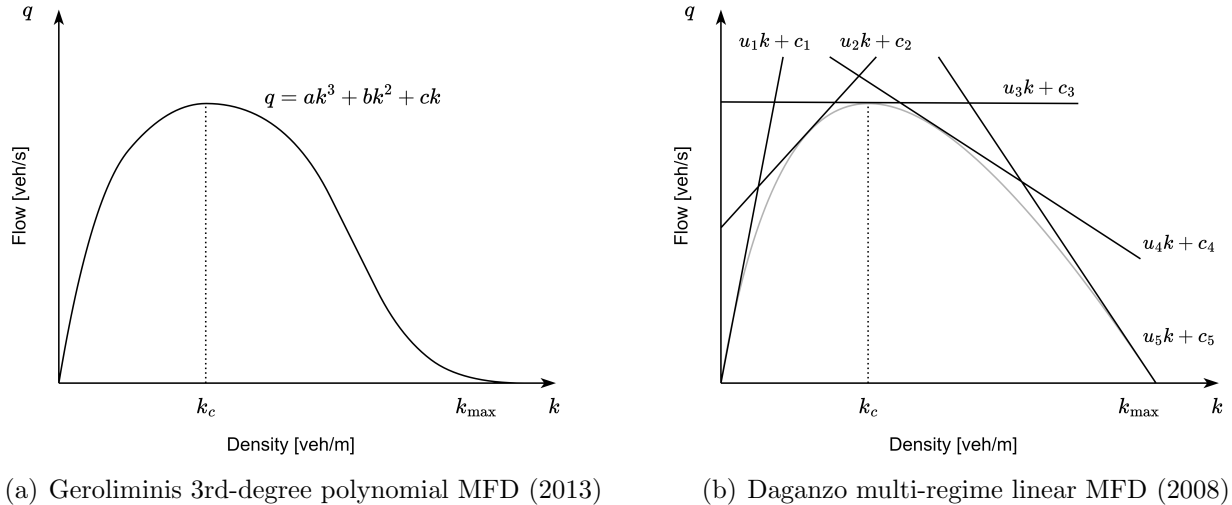


Figure 2: Mathematical models of MFDs

2013), as shown in Eq. 2a and Eq. 2b. The advantage of using an $m - n$ MFD is that it can serve as a transfer function to deduce the future system dynamics, which is particularly common practice in the study of various traffic control strategies, as in (Rodrigues and Azevedo, 2019; Zhou and Gayah, 2021; Genser and Kouvelas, 2022).

$$n = kD \quad (2a)$$

$$m = \frac{qD}{L} \quad (2b)$$

3. Problem formulation

In this study, we focus on the relationship between vehicle time spent versus disruption magnitudes, following a loss-disruption relationship, however, a bigger picture of (anti-)fragility as shown in Fig. 3 can help facilitate the understanding of the gist behind it. In this four-quadrant diagram, while the first quadrant shows a gain-opportunity relationship, the third quadrant illustrates the loss-disruption relationship, which is the focus of the study. Although convexity signifies an antifragile response on the whole four-quadrant diagram, when it comes to each quadrant, convexity or concavity itself does not necessarily indicate (anti-)fragility without the context. Also, a variable can be an opportunity for one indicator but becomes a disruption for another. For example, while traffic density always imposes a non-positive effect on travel speed and thus follows the loss-disruption relationship with the fragile response being convex, vehicle accumulation can actually be beneficial to trip completion so that the related fragility curve is concave. In our case, as highlighted in the beige color, both nonlinear functions can be represented by Jensen's inequality, with either $E[g(X)] \geq g(E[X])$ for a fragile response or $E[g(X)] \leq g(E[X])$ for an antifragile response. This relationship can then be determined through the second derivative (Ruel et al., 1999), i.e., a positive second derivative featuring a convex function and hence a fragile system and vice versa. It should be noted that the calculation of the derivatives is only possible when the function is continuous and differentiable, which means the underlying mathematical model representing the system needs to be known beforehand.

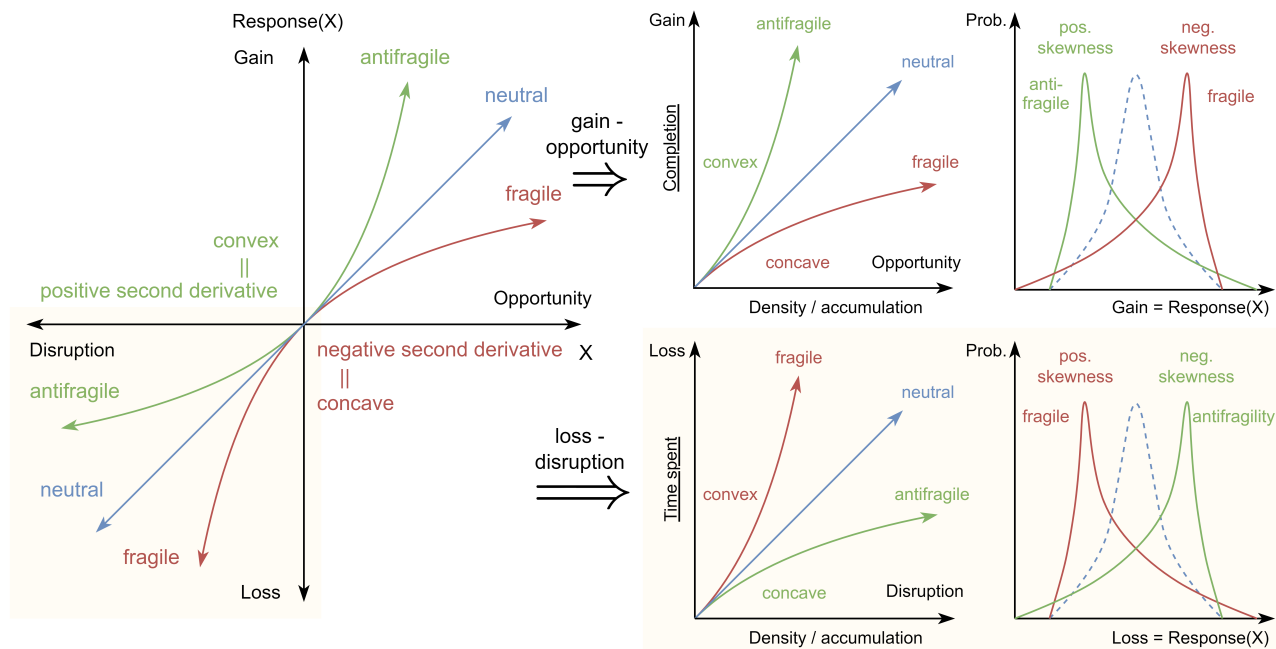


Figure 3: Antifragility in a four-quadrant diagram

However, in most real-world scenarios, the mathematical function of the system is agnostic, and only discrete measurements of the system's performance are available. In this case, we can calculate the distribution skewness to determine the (anti-)fragile property of the system, as illustrated with an example of financial deficit in [Taleb and Douady \(2013\)](#) and [Coppitters and Contino \(2023\)](#) when designing an antifragile renewable energy system. For a loss-disruption relationship, a positive skewness represented by the long tail pointing to the left indicates a fragile response, whereas a negative skewness showcases the fragility of a gain-opportunity relationship.

For the following mathematical analysis of the fragile nature of road transportation systems under a unified framework, we address three sets of opposing concepts:

- link level / network level
- demand disruption / supply disruption
- onset of disruption / recovery from disruption

As link-level and network-level traffic models were introduced in the previous [Section 2](#), we start with differentiating between demand and supply disruptions. Since traffic networks primarily involve the management of supply and demand, any traffic disruption in the real world can be classified as either a demand or a supply disruption. A demand disruption can be easily understood as, for example, surging traffic due to a social event, whereas a supply disruption may indicate an impaired network due to external factors, such as adversarial weather or lane closure. Additionally, since disruptions represent abnormal cases that only exist temporarily, we consider not only the onset of disruptions but also assess the recovery process of the systems following such disruptions. This coincides with the definitions of robustness and resilience, i.e., robustness is about resistance against disruptions while resilience is about the recovery from them. By considering both the onset and the recovery processes, it is possible to compare the performance between either robust and antifragile designs or resilient and antifragile designs. The scheme

of onset and recovery from demand or supply disruptions are illustrated in Fig. 4(a) and Fig. 4(b), and since FDs share similar profiles as MFDs, we use MFDs here as generic examples for illustration.

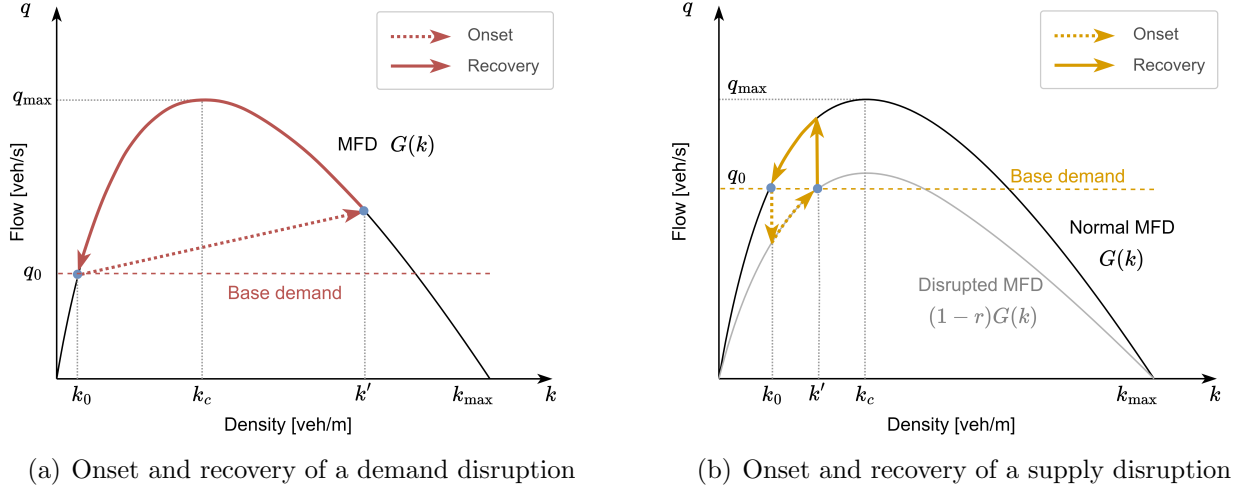


Figure 4: Onset and recovery of disruptions

We denote the FD/MFD profile as $G(k)$ and assume a constant base demand in the network as q_0 , resulting in an equilibrium traffic state without any disruption. The initial density at equilibrium, the critical density, the new density after disruption, and the gridlock density are denoted as k_0 , k_c , k' , and k_{\max} , respectively. For the study of supply disruptions, we introduce a disruption magnitude coefficient, denoted as r , so that the disrupted MFD profile can be represented by $(1-r)G(k)$. It should also be noted that at the network level, MFD can also be represented with the vehicle accumulation – trip completion relationship instead of the flow – density relationship. Hence, with vehicle accumulation denoted as n , k' and $G(k)$ can also be replaced with n' and trip completion $M(n)$. For clarity, a notation list is summarized in Table 1. Another separate table of notations with real-world values solely for the numerical simulation can be found in Section 6.

Several assumptions need to be established to define the scope of our work. As the study of fragility involves the recovery process from disruptions, a critical condition to avoid here is the network succumbing to a complete gridlock, where recovery is not possible anymore.

Assumption 1. *We study the onset of disruptions focusing only on the stable traffic state after the disruptions, while the recovery is regarded as a gradual process of congestion dissipation.*

For the onset of demand disruptions, we assume a rapid influx of traffic into the network, which can be characterized as an instantaneous shift of the equilibrium point in blue as shown in Fig. 4(a). For the onset of supply disruptions, although it may take some time for the number of vehicles within the network to accumulate, we also understand it as an instantaneous change from the original stable traffic state $q_0 = G(k_0)$ to the new stable state $q_0 = (1-r)G(k')$ after disruption. On the other hand, the recovery process from demand or supply disruptions takes significantly longer as it is a traffic unloading and congestion dissipation process instead of an instantaneous event.

Assumption 2. *We assume the disruption density is greater than the critical density $k' > k_c$ for demand disruptions, whereas $k' < k_c$ for supply disruptions.*

Table 1: List of notations

FD/MFD-related notations			
N	Total number of cuts according to MoC		
y	Starting cut (the most congested cuts)		
z	Ending cut (the least congested cuts)		
i	Sequential number of cuts from the most to the least congested cuts		
<u>Flow - density</u>		<u>Trip completion - accumulation</u>	
$G(\cdot)$	Functional form of FD/MFD	$M(\cdot)$	Functional form of MFD
k	Density	n	Vehicle accumulation
k_c	Critical density	n_c	Critical vehicle accumulation
k_{\max}	Maximal density at gridlock	n_{\max}	Maximal accumulation at gridlock
k_0	Initial density at equilibrium	n_0	Initial accumulation at equilibrium
k'	Disruption density	n'	Disruption vehicle accumulation
q	Traffic flow	m	Trip completion
q_{\max}	Capacity of the network, $k = k_c$	m_{\max}	Maximal trip completion, $n = n_c$
q_0	Base demand flow, $k = k_0$	m_0	Base demand inflow, $n = n_0$
q'	Flow on disruption density, $k = k'$	m'	Completion at disruption, $n = n'$
v	Speed, $v = q/k$	a	Completion rate, $a = m/n$
u_i	Gradient of cut i	a_i	Gradient of cut i
c_i	Intercept of cut i	b_i	Intercept of cut i
u_f	Free flow speed, $u_f = u_N$	a_f	Gradient of the free flow cut
w	Backward wave speed, $w = u_1$	a_w	Gradient of the backward wave cut
$n_{\bar{c},i}, m_{\bar{c},i}$	Critical accumulation and completion between cut i and cut $i + 1$ according to MoC		
$n_{\bar{c}}, m_{\bar{c}}$	Critical accumulation and completion of the virtual interception between cut y and cut z		
$\alpha_3, \alpha_2, \alpha_1$	Generic coefficients for polynomial FD/MFD, e.g., $G(k) = \alpha_3 k^3 + \alpha_2 k^2 + \alpha_1 k^1$		
Other notations			
L	Average trip length		
l	Average lane length		
D	Total lane length of a network		
r	Supply disruption magnitude coefficient		
t	Time		
t_c	Time to reach critical density/accumulation		
$t_{\bar{c},i}$	Time to reach critical density/accumulation between cut i and cut $i + 1$		

A surging demand should be considered a disruption only when the traffic state $(k', G(k'))$ enters the congested zone of the MFD with $k' > k_c$, causing a reduction in the network's maximal possible serviceability. On the other hand, for supply disruption under the constant base demand q_0 , if the traffic state can ever surpass the maximal capacity of the disrupted MFD profile, i.e., $k' > k_c$, indicating that q_0 has to be greater than the disrupted maximal capacity of the network $(1-r)q_{\max}$. In this case, the traffic density will continue to accumulate until the network reaches a full gridlock, and there will be no equilibrium point in this case after a disruption, violating

Assumption 1.

Assumption 3. *We assume the base demand $q_0 < G(k')$ for demand disruption, whereas $q_0 < (1 - r)G(k_c)$ for supply disruptions.*

Likewise, this assumption also lies in avoiding gridlock for both demand and supply disruptions. If the base demand q_0 is higher than the outflow $G(k')$ after a demand disruption or the maximal capacity of the network $(1 - r)G(k_c)$ after a supply disruption, then the traffic state will continue to move to complete gridlock $(k_{\max}, 0)$.

4. Mathematical analysis of the fragility of road transportation systems

In this section, we conduct a mathematical analysis to evaluate the potential fragility of road transportation systems at both link and network levels. The structure of this section is summarized in Table 2. The reason for not considering the recovery process at the link level is that researchers rarely use FDs to study the recovery from congestion for a link section. And even if we do so, we can also easily get the same conclusion with Proposition 3 and Proposition 6. In the subsequent study, to investigate the instantaneous disruption onset between different stable states, the Average Time Spent (ATS) serves as the indicator for the overall performance of a link or a network, since ATS remains constant at any stable traffic state. Conversely, for the examination of disruption recovery, we use Total Time Spent (TTS), as applied in [Rodrigues and Azevedo \(2019\)](#); [Zhou and Gayah \(2021\)](#); [Chen et al. \(2022\)](#), to better reflect the temporal costs for all vehicles in the process, considering that the time spent in the network varies significantly for vehicles entering at different times.

Table 2: Structure of the mathematical proof

Disruption	Demand		Supply	
	Link	Network	Link	Network
Onset	Proposition 1	Proposition 2	Proposition 4	Proposition 5
Recovery	-	Proposition 3	-	Proposition 6

4.1. Demand disruption

As outlined in Section 3, the presence of a positive second derivative in performance loss regarding the magnitude of disruption serves as an indication of the transportation system’s fragility. Therefore, to illustrate the system’s fragility to demand disruption, we analyze the derivatives of time spent, namely ATS for the onset of disruptions or TTS for the recovery process, relative to the initial disruption demand, either represented by disruption density k' or an initial disruption demand n' when we study the relationship between trip completion and vehicle accumulation. If the system is neither fragile nor antifragile, this approach is expected to yield a linearly growing loss in performance alongside the disruption and zero derivatives. Regarding the traffic models to be selected, numerical forms of FD/MFD have the strength of generally being considered more accurate as they are directly approximated from mass sensor data with algebraic functions such as polynomials or exponential functions. On the other hand,

analytical forms of FDs/MFD are derived from parameters with physical meanings like capacity and free flow speed without the presence of sensor data, allowing for the estimate of the traffic model with the least amount of information and costs for sensor installation. Therefore, we employ both a numerical and an analytical FD/MFD to investigate the fragile properties under the onset of demand disruption at the link level and the whole network.

Proposition 1. *Road transportation systems are fragile with the onset of demand disruptions at the link level.*

Proof. We choose the second-degree polynomial FD in [Greenshields et al. \(1934\)](#) as the numerical traffic model and the two-regime linear FD in [Daganzo \(1994\)](#) as the analytical traffic model.

For the Greenshields second-degree polynomial FD, the following equations describe traffic in a stable state with α_1 and α_2 being the polynomial coefficients. The traffic flow q and average speed v can be determined as in Eq. 3a and Eq. 3b, with the speed-density profile shown in Fig. 5(a).

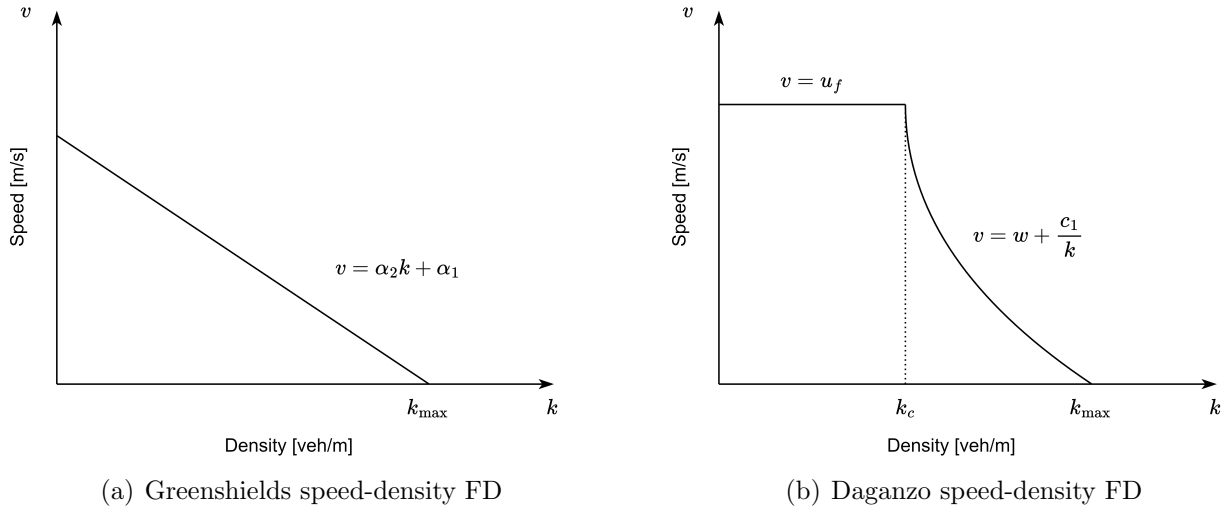


Figure 5: Mathematical models of speed-density FDs

$$G(k) = \alpha_2 k^2 + \alpha_1 k \quad (3a)$$

$$v(k) = \frac{q}{k} = \alpha_2 k + \alpha_1 \quad (3b)$$

With the sudden onset of a demand disruption k' , for a link with a given length of l , the ATS and its first and second derivatives over such disruption density k' are:

$$ATS = \frac{l}{v(k')} = \frac{l}{\alpha_2 k' + \alpha_1} \quad (4a)$$

$$\frac{dATS}{dk'} = -\alpha_2 (\alpha_2 k' + \alpha_1)^{-2} l \quad (4b)$$

$$\frac{d^2 ATS}{dk'^2} = 2\alpha_2^2 (\alpha_2 k' + \alpha_1)^{-3} l \quad (4c)$$

Since the coefficient α_2 is negative and the physical meaning of the term $\alpha_2 k' + \alpha_1$ is the average speed of vehicles at this link, which should always be positive until reaching gridlock, both the first and second derivatives of ATS over k' are positive, indicating the fragility of transportation systems at a link level.

In the Daganzo two-regime linear model, the speed-density FD can be formulated as the following Eq. 5, as shown in Fig. 5(b).

$$v(k) = \begin{cases} u_f, & 0 \leq k < k_c \\ w + \frac{c_1}{k}, & k_c \leq k < k_{\max} \end{cases} \quad (5)$$

When the disruption density k' is below the critical density k_c , the ATS and its first and second derivatives are:

$$ATS = \frac{l}{u_f} \quad (6a)$$

$$\frac{dATS}{dk'} = 0 \quad (6b)$$

$$\frac{d^2ATS}{dk'^2} = 0 \quad (6c)$$

The second derivative being zero indicates that the traffic states before k_c are neither fragile nor antifragile. However, as per Assumption 2, the congested area of the MFD is the study focus for demand disruptions, so now we study the derivatives when k' is over k_c :

$$ATS = \frac{l}{v(k')} = \frac{l}{w + \frac{c_1}{k'}} \quad (7a)$$

$$\frac{dATS}{dk'} = \frac{c_1 l}{(wk' + c_1)^2} \quad (7b)$$

$$\frac{d^2ATS}{dk'^2} = \frac{-2wc_1 l}{(wk' + c_1)^3} \quad (7c)$$

Before the disruption density k' reaches the maximal density k_{\max} of this link, $wk' + c_1 > 0$ always holds true, and since $w < 0$ as well as $c_1 > 0$, therefore, both the first and second derivatives are positive. □

Proposition 2. *Road transportation systems are fragile with the onset of demand disruptions at the network level.*

Proof. Likewise, at the network level, we study the fragile property based on the third-degree polynomial MFD in Geroliminis et al. (2013) and multi-regime linear MFD based on MoC in Daganzo and Geroliminis (2008). For MFD approximated with a third-degree polynomial, similar to the Greenshields FD in Eq. 3a, we have:

$$G(k) = \alpha_3 k^3 + \alpha_2 k^2 + \alpha_1 k \quad (8a)$$

$$v(k) = \frac{q}{k} = \alpha_3 k^2 + \alpha_2 k + \alpha_1 \quad (8b)$$

Consequently, the ATS and its first and second derivatives are:

$$ATS = \frac{l}{v(k')} = \frac{l}{\alpha_3 k'^2 + \alpha_2 k' + \alpha_1} \quad (9a)$$

$$\frac{dATS}{dk'} = \frac{-(2\alpha_3 k' + \alpha_2)l}{(\alpha_3 k'^2 + \alpha_2 k' + \alpha_1)^2} \quad (9b)$$

$$\frac{d^2 ATS}{dk'^2} = \frac{\frac{3}{2}(2\alpha_3 k' + \alpha_2)^2 + \frac{1}{2}(\alpha_2^2 - 4\alpha_1\alpha_3)l}{(\alpha_3 k'^2 + \alpha_2 k' + \alpha_1)^3} \quad (9c)$$

The average speed has to be a real number, indicating Eq. 8b should have real roots, so $\alpha_2^2 - 4\alpha_1\alpha_3 > 0$ should hold true. Thus, since $\alpha_3 k'^2 + \alpha_2 k' + \alpha_1$ represents the speed and is therefore positive, the derivatives are also positive.

The MFD derived from MoC can be approximated with a series of linear functions. Likewise to the Daganzo two-regime linear FD as in Eq. 7c, for any linear function, the second derivative is:

$$\frac{d^2 ATS}{dk'^2} = \frac{-2u_i c_i l}{(u_i k' + c_i)^3} \quad (10)$$

As coefficient c_i is non-negative for any cut i since the y-intercept should always be non-negative by definition of MoC, whether the second derivative is positive or negative depends solely on u_i . The cuts that intercept the MFD before the critical density k_c exhibit antifragile properties ($u_i > 0$, in blue as shown in Fig. 6) while the others with intercepts larger than the critical density k_c show fragile responses ($u_i < 0$, in red), with an exception in case there's a cut at the critical density ($u_i = 0$, in gray). Conforming to Assumption 2, for demand disruptions, we focus on the cuts with intercepts larger than the critical density k_c ($u_i < 0$). The second derivative for these cuts is positive indicating a fragile property.

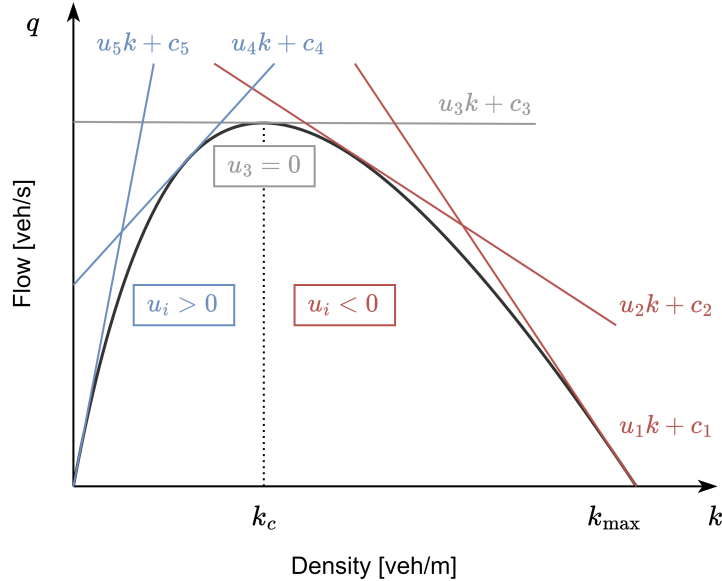


Figure 6: Daganzo multi-regime linear MFD

□

Proposition 3. *Road transportation systems are fragile when going through the recovery process from demand disruptions.*

Proof. The MoC is composed of a series of linear functions, which are referred to as cuts $1, 2, \dots, N$, with increasing gradients as the vehicle accumulation decreases, and such multi-linear regimes are presented in Fig. 7, where the black dashed lines indicate multiple cuts for simplicity. For a given cut i , the slope and the y-intercept on the coordinates are denoted as a_i and b_i , with $a_{i+1} > a_i$ and $b_i > b_{i+1} > 0$. The critical accumulation $n_{\bar{c},i}$ on the x -axis does not represent the critical point of the entire MFD, but rather the critical accumulation between any two consecutive cuts i and $i + 1$ with two exceptional cases being $n_{\bar{c},0} = n_{\max}$ and $n_{\bar{c},N} = 0$. According to Assumption 1, we simplify this surging demand as a disruption that takes place instantly in the network, denoted as n' at time $t_0 = 0$ and lands on cut y . At time $t_{\bar{c},i}$ ($y \leq i < z$), the number of vehicles in the network reaches this critical accumulation $n_{\bar{c},i}$. And after any period t , the traffic state lands on the cut z . A virtual intersection point $(n_{\bar{c}}, m_{\bar{c}})$ between cut y and cut z is also illustrated and will be discussed later in this section. We also denote the initial trip completion and critical trip completion as $m' = a_y n' + b_y$ and $m_{\bar{c},i} = a_i n_{\bar{c},i} + b_i = a_{i+1} n_{\bar{c},i} + b_{i+1}$ respectively.

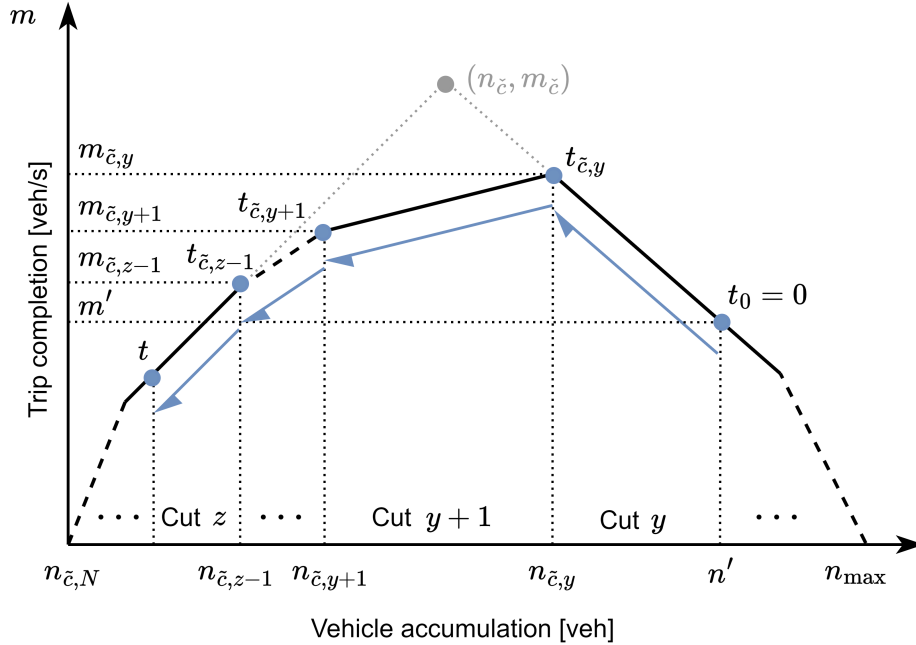


Figure 7: Simplification of MoC

Any cut i of the MFD can be formulated into the following Eq. 11:

$$M(n) = a_i n + b_i, \forall n \in (n_{\bar{c},i}, n_{\bar{c},i-1}] \quad (11)$$

By calculating the difference between the base demand m_0 as the inflow rate and the trip completion $M(n)$ as the outflow rate, the system dynamics on cut i can be summarized as Eq. 12:

$$\frac{dn}{d\tau} = -M(n) + m_0 = -a_i n - b_i + m_0 \quad (12)$$

Assuming that the traffic states move only along a single cut i , and with any amount of vehicle accumulation n_1 at the beginning of a given period between t_1 and t_2 , the number of vehicles n_2 at the end of this period t can be determined as:

$$\int_{t_1}^{t_2} d\tau = - \int_{n_1}^{n_2} \frac{1}{a_i n + b_i - m_0} dn \quad (13a)$$

$$\implies t_2 - t_1 = -\frac{1}{a_i} \ln \left(\frac{a_i n_2 + b_i - m_0}{a_i n_1 + b_i - m_0} \right) \quad (13b)$$

$$\implies n_2 = \frac{e^{-a_i(t_2-t_1)}(a_i n_1 + b_i - m_0)}{a_i} - \frac{b_i - m_0}{a_i} \quad (13c)$$

Therefore, with the disruption accumulation n' , and when the traffic states are assumed to be on the same cut i . After any time t , the vehicle accumulation n would be:

$$n = \frac{a_i n' + b_i - m_0}{a_i} e^{-a_i t} - \frac{b_i - m_0}{a_i} \quad (14)$$

The TTS on this cut i for a given period t can be calculated as:

$$\begin{aligned} TTS &= \int_0^t n d\tau = \int_0^t \left(\frac{a_i n' + b_i - m_0}{a_i} e^{-a_i \tau} - \frac{b_i - m_0}{a_i} \right) d\tau \\ &= -\frac{a_i n' + b_i - m_0}{a_i^2} e^{-a_i t} - \frac{b_i - m_0}{a_i} t + \frac{a_i n' + b_i - m_0}{a_i^2} \end{aligned} \quad (15)$$

Now we calculate the derivatives of TTS assuming $t < t_{\bar{c},i}$.

$$\frac{dTTS}{dn'} = \frac{1}{a_i} - \frac{e^{-a_i t}}{a_i} \quad (16a)$$

$$\frac{d^2 TTS}{dn'^2} = 0 \quad (16b)$$

The second derivative of TTS is 0, indicating that when the traffic states move only along a single cut i , it shows neither fragility nor antifragility. On the other hand, when the traffic state goes over the critical vehicle accumulation $n_{\bar{c},i}$, and since the MoC is a piecewise function, we calculate the TTS and the related derivatives separately on each concerned cut $y, y+1, \dots, z$, denoted as $TTS_y, TTS_{y+1}, \dots, TTS_z$. Since the critical time $t_{\bar{c},i}$ is yet unknown, we need to determine $t_{\bar{c},i}$ first based on Eq. 13b.

$$t_{\bar{c},y} = -\frac{1}{a_y} \ln \left(\frac{a_y n_{\bar{c},y} + b_y - m_0}{a_y n' + b_y - m_0} \right) \quad (17a)$$

$$t_{\bar{c},y+1} - t_{\bar{c},y} = -\frac{1}{a_{y+1}} \ln \left(\frac{a_{y+1} n_{\bar{c},y+1} + b_{y+1} - m_0}{a_{y+1} n_{\bar{c},y} + b_{y+1} - m_0} \right) \quad (17b)$$

⋮

$$t_{\bar{c},z-1} - t_{\bar{c},z-2} = -\frac{1}{a_{z-1}} \ln \left(\frac{a_{z-1} n_{\bar{c},z-1} + b_{z-1} - m_0}{a_{z-1} n_{\bar{c},z-2} + b_{z-1} - m_0} \right) \quad (17c)$$

Therefore, the time $t_{\bar{c},z-1}$ to reach the last critical point $n_{\bar{c},z-1}$ is:

$$t_{\bar{c},z-1} = -\frac{1}{a_y} \ln \left(\frac{a_y n_{\bar{c},y} + b_y - m_0}{a_y n' + b_y - m_0} \right) - \sum_{i=y+1}^{z-1} \frac{1}{a_i} \ln \left(\frac{a_i n_{\bar{c},i} + b_i - m_0}{a_i n_{\bar{c},i-1} + b_i - m_0} \right) \quad (18)$$

As $a_y n_{\bar{c},y} + b_y$ is equal to $m_{\bar{c},y}$, we can rewrite the above Eq. 17a as:

$$t_{\bar{c},y} = -\frac{1}{a_y} \ln \left(\frac{m_{\bar{c},y} - m_0}{a_y n' + b_y - m_0} \right) \quad (19)$$

A generalized form between any two consecutive critical points $n_{\bar{c},i-1}$ and $n_{\bar{c},i}$ will be:

$$t_{\bar{c},i} - t_{\bar{c},i-1} = -\frac{1}{a_i} \ln \left(\frac{m_{\bar{c},i} - m_0}{m_{\bar{c},i-1} - m_0} \right) \quad (20)$$

Similarly, the above Eq. 18 can also be rewritten as:

$$t_{\bar{c},z-1} = -\frac{1}{a_y} \ln \left(\frac{m_{\bar{c},y} - m_0}{a_y n' + b_y - m_0} \right) - \sum_{i=y+1}^{z-1} \frac{1}{a_i} \ln \left(\frac{m_{\bar{c},i} - m_0}{m_{\bar{c},i-1} - m_0} \right) \quad (21)$$

We substitute t in Eq. 15 with $t_{\bar{c},y}$ in Eq. 19, and the TTS_y for the more congested cut will be:

$$\begin{aligned} TTS_y &= \int_0^{t_{\bar{c},y}} n d\tau = -\frac{a_y n' + b_y - m_0}{a_y^2} e^{-a_y t_{\bar{c},y}} - \frac{b_y - m_0}{a_y} t_{\bar{c},y} + \frac{a_y n' + b_y - m_0}{a_y^2} \\ &= -\frac{m_{\bar{c},y} - m_0}{a_y^2} + \frac{b_y - m_0}{a_y^2} \ln \left(\frac{m_{\bar{c},y} - m_0}{a_y n' + b_y - m_0} \right) + \frac{a_y n' + b_y - m_0}{a_y^2} \end{aligned} \quad (22)$$

The derivatives for TTS_y are:

$$\frac{dTTS_y}{dn'} = -\frac{b_y - m_0}{a_y} (a_y n' + b_y - m_0)^{-1} + \frac{1}{a_y} \quad (23a)$$

$$\frac{d^2 TTS_y}{dn'^2} = (b_y - m_0) (a_y n' + b_y - m_0)^{-2} \quad (23b)$$

Now we consider the cuts between the most congested cut y and the least congested cut z . Combining Eq. 13c and Eq. 15, the TTS_i on any cut $y < i < z$ is:

$$\begin{aligned} TTS_i &= \int_{t_{\bar{c},i-1}}^{t_{\bar{c},i}} n d\tau = \int_{t_{\bar{c},i-1}}^{t_{\bar{c},i}} \left(\frac{e^{-a_i(\tau - t_{\bar{c},i-1})} (a_i n_{\bar{c},i-1} + b_i - m_0)}{a_i} - \frac{b_i - m_0}{a_i} \right) d\tau \\ &= -\frac{e^{-a_i(t_{\bar{c},i} - t_{\bar{c},i-1})} (m_{\bar{c},i-1} - m_0)}{a_i^2} + \frac{(m_{\bar{c},i-1} - m_0)}{a_i^2} - \frac{b_i - m_0}{a_i} (t_{\bar{c},i} - t_{\bar{c},i-1}) \end{aligned} \quad (24)$$

Then $t_{\bar{c},i} - t_{\bar{c},i-1}$ can be substituted with Eq. 20:

$$TTS_i = -\frac{m_{\bar{c},i} - m_{\bar{c},i-1}}{a_i^2} + \frac{b_i - m_0}{a_i^2} \ln \left(\frac{m_{\bar{c},i} - m_0}{m_{\bar{c},i-1} - m_0} \right) \quad (25)$$

As Eq. 25 is not dependent on n' . Therefore, the second derivative of TTS_i over n' with $y < i < z$ are:

$$\frac{dTTS_i}{dn'} = 0 \quad (26a)$$

$$\frac{d^2TTS_i}{dn'^2} = 0 \quad (26b)$$

The final piece of the puzzle is the least congested cut z , and likewise to Eq. 24, the TTS_z is:

$$TTS_z = -\frac{e^{-a_z(t-t_{\bar{c},z-1})}(m_{\bar{c},z-1} - m_0)}{a_z^2} + \frac{(m_{\bar{c},z-1} - m_0)}{a_z^2} - \frac{b_z - m_0}{a_z}(t - t_{\bar{c},z-1}) \quad (27)$$

We substitute $t_{\bar{c},z-1}$ with Eq. 21:

$$\begin{aligned} TTS_z = & -\frac{e^{-a_z t}}{a_z^2}(m_{\bar{c},z-1} - m_0) \left(\frac{m_{\bar{c},y} - m_0}{a_y n' + b_y - m_0} \right)^{-\frac{a_z}{a_y}} \prod_{i=y+1}^{z-1} \left(\frac{m_{\bar{c},i} - m_0}{m_{\bar{c},i-1} - m_0} \right)^{-\frac{a_z}{a_i}} + \frac{(m_{\bar{c},z-1} - m_0)}{a_z^2} \\ & - \frac{b_z - m_0}{a_z} \left(t + \frac{1}{a_y} \ln \left(\frac{a_y n_{\bar{c},y} + b_y - m_0}{a_y n' + b_y - m_0} \right) + \sum_{i=y+1}^{z-1} \frac{1}{a_i} \ln \left(\frac{a_i n_{\bar{c},i} + b_i - m_0}{a_i n_{\bar{c},i-1} + b_i - m_0} \right) \right) \end{aligned} \quad (28)$$

A constant P is introduced for conciseness since all the parameters involved below are constants:

$$P = (m_{\bar{c},y} - m_0)^{-\frac{a_z}{a_y}} \prod_{i=y+1}^{z-1} \left(\frac{m_{\bar{c},i} - m_0}{m_{\bar{c},i-1} - m_0} \right)^{-\frac{a_z}{a_i}} \quad (29)$$

The derivatives for the least congested cut z are:

$$\frac{dTTS_z}{dn'} = -\frac{e^{-a_z t} P}{a_z} (m_{\bar{c},z-1} - m_0) (a_y n' + b_y - m_0)^{\frac{a_z}{a_y} - 1} + \frac{b_z - m_0}{a_z} (a_y n' + b_y - m_0)^{-1} \quad (30a)$$

$$\frac{d^2TTS_z}{dn'^2} = -\left(\frac{e^{-a_z t} P}{a_z} (a_z - a_y) (m_{\bar{c},z-1} - m_0) (a_y n' + b_y - m_0)^{\frac{a_z}{a_y}} + \frac{a_y (b_z - m_0)}{a_z} \right) (a_y n' + b_y - m_0)^{-2} \quad (30b)$$

The second derivative of the whole process is the sum of the second derivatives for the sub-process on each cut, as calculated in Eq. 23b, Eq. 26b, and Eq. 30b:

$$\begin{aligned}
\frac{d^2TTS}{dn'^2} &= \frac{d^2TTS_y}{dn'^2} + \sum_{i=y+1}^{z-1} \frac{d^2TTS_i}{dn'^2} + \frac{d^2TTS_z}{dn'^2} \\
&= \left(b_y - m_0 - \frac{e^{-a_z t} P}{a_z} (a_z - a_y) (m_{\tilde{c}, z-1} - m_0) (m' - m_0)^{\frac{a_z}{a_y}} - \frac{a_y (b_z - m_0)}{a_z} \right) (m' - m_0)^{-2}
\end{aligned} \tag{31}$$

As per Assumption 3, it is assumed that $m' - m_0 > 0$, so if a transportation system is to be fragile, $\frac{d^2TTS}{dn'^2}$ should be positive, and the following equation has to be proven to be true:

$$b_y - m_0 - \frac{e^{-a_z t} P}{a_z} (a_z - a_y) (m_{\tilde{c}, z-1} - m_0) (m' - m_0)^{\frac{a_z}{a_y}} - \frac{a_y (b_z - m_0)}{a_z} > 0 \tag{32}$$

Since $t > t_{\tilde{c}, z-1}$, regardless of whether a_z is positive or negative, the below relationship always holds:

$$-\frac{e^{-a_z t}}{a_z} > -\frac{e^{-a_z t_{\tilde{c}, z-1}}}{a_z} \tag{33}$$

As all of the following terms: P , $a_z - a_y$, $m_{\tilde{c}, z-1} - m_0$, and $(m' - m_0)^{\frac{a_z}{a_y}}$, are all positive, the following relationship is true:

$$\begin{aligned}
b_y - m_0 - \frac{e^{-a_z t} P}{a_z} (a_z - a_y) (m_{\tilde{c}, z-1} - m_0) (m' - m_0)^{\frac{a_z}{a_y}} - \frac{a_y (b_z - m_0)}{a_z} &> \\
b_y - m_0 - \frac{e^{-a_z t_{\tilde{c}, z-1}} P}{a_z} (a_z - a_y) (m_{\tilde{c}, z-1} - m_0) (m' - m_0)^{\frac{a_z}{a_y}} - \frac{a_y (b_z - m_0)}{a_z} &>
\end{aligned} \tag{34}$$

We substitute $t_{\tilde{c}, z-1}$ in Eq. 34 with Eq. 21 and constant P with Eq. 29 and here goes:

$$b_y - m_0 - \frac{(a_z - a_y) (m_{\tilde{c}, z-1} - m_0)}{a_z} - \frac{a_y (b_z - m_0)}{a_z} = b_y - m_{\tilde{c}, z-1} - \frac{a_y}{a_z} (b_z - m_{\tilde{c}, z-1}) \tag{35}$$

$m_{\tilde{c}, z-1}$ can be substituted by $a_z n_{\tilde{c}, z-1} + b_z$, so it further becomes:

$$b_y - a_z n_{\tilde{c}, z-1} - b_z - \frac{a_y}{a_z} (b_z - a_z n_{\tilde{c}, z-1} - b_z) = b_y - b_z + (a_y - a_z) n_{\tilde{c}, z-1} \tag{36}$$

Since $z > y$, so both $b_y > b_z$ and $a_y < a_z$ hold true. Also, if cut y and cut z are consecutive, i.e., $z = y + 1$, the virtual intersection point exists physically $n_{\tilde{c}} = n_{\tilde{c}, z-1}$. Otherwise, when there is any other cut in between, then $n_{\tilde{c}} > n_{\tilde{c}, z-1}$ holds. Therefore, it can be formulated as $n_{\tilde{c}} \geq n_{\tilde{c}, z-1}$ and we define a non-negative value $\Delta n = n_{\tilde{c}} - n_{\tilde{c}, z-1}$ so that Eq. 36 can be rewritten as:

$$\begin{aligned}
b_y - b_z + (a_y - a_z)(n_{\bar{c}} - \Delta n) &= (a_y n_{\bar{c}} + b_y) - (a_z n_{\bar{c}} + b_z) - (a_y - a_z)\Delta n \\
&= m_{\bar{c}} - m_{\bar{c}} - (a_y - a_z)\Delta n \geq 0
\end{aligned} \tag{37}$$

Having demonstrated its lower bound to be non-negative, it is certain that:

$$\frac{d^2 TTS}{dn'^2} = \left(b_y - m_0 - \frac{e^{-a_z t} P}{a_z} (a_z - a_y)(m_{\bar{c}, z-1} - m_0)(m' - m_0)^{\frac{a_z}{a_y}} - \frac{a_y(b_z - m_0)}{a_z} \right) (m' - m_0)^{-2} > 0 \tag{38}$$

The second derivative of TTS over the disruption vehicle accumulation n' is positive, which indicates the fragility. \square

4.2. Supply disruption

While a positive second derivative of ATS or TTS on traffic demand signifies the fragility of the road transportation network to demand disruptions, establishing a positive second derivative of time spent concerning the magnitude of FD/MFD disruption would demonstrate the fragility from the perspective of supply disruptions. Here we use a supply disruption magnitude coefficient r and the disrupted FD/MFD is expressed as $(1 - r)G(n)$. Although real-world MFD may be decreased in various shapes, we use this simple approach as applied in [Ambühl et al. \(2020\)](#) when studying the uncertainties of MFDs. The physical meaning of $(1 - r)G(n)$ relates to the decrease of the free-flow speed due to, e.g., snowy weather and icy roads, with the maximal density of the network remaining unchanged. The traffic demand at equilibrium before the MFD disruption is $q_0 = G(k_0)$, or $m_0 = M(n_0)$. After the supply disruption, as per Assumption 3, the supply disruption magnitude coefficient $r \in [0, 1)$ is not significantly large so the traffic demand remains below the maximal capacity on the disrupted MFD profile, and the new equilibrium point is $q_0 = (1 - r)G(k'(r))$, or $m_0 = (1 - r)M(n'(r))$. It should be noted that, unlike the study of demand disruption, when studying supply disruptions, $k'(r)$ is a dependent variable on r .

Proposition 4. *Road transportation systems are fragile with the onset of supply disruptions at the link level.*

Proof. First, we study the fragile properties of the road transportation systems under the onset of supply disruptions based on the link-level Greenshields FD. Here, the base demand q_0 is constant before and after the onset of the supply disruption, and can be used to build the relationship between the two stable states before and after the supply disruption.

$$q_0 = G(k_0) = (1 - r)G(k'(r)) = (1 - r)(\alpha_2 k'(r)^2 + \alpha_1 k'(r)) \tag{39}$$

So, the traffic density of the new equilibrium point after the supply disruption would be:

$$k'(r) = \frac{\sqrt{\alpha_1^2 + \frac{4\alpha_2 q_0}{1-r}} - \alpha_1}{2\alpha_2} \tag{40}$$

The ATS and its first and second derivatives are:

$$ATS = \frac{l}{v(k')} = \frac{lk'(r)}{q_0} = \frac{l}{2\alpha_2 q_0} \left((\alpha_1^2 + \frac{4\alpha_2 q_0}{1-r})^{\frac{1}{2}} - \alpha_1 \right) \quad (41a)$$

$$\frac{dATS}{dr} = l(\alpha_1^2(1-r) + 4\alpha_2 q_0)^{-\frac{1}{2}}(1-r)^{-\frac{3}{2}} \quad (41b)$$

$$\frac{d^2ATS}{dr^2} = \frac{\alpha_1^2 l}{2} (\alpha_1^2(1-r) + 4\alpha_2 q_0)^{-\frac{3}{2}}(1-r)^{-\frac{3}{2}} + \frac{3l}{2} (\alpha_1^2(1-r) + 4\alpha_2 q_0)^{-\frac{1}{2}}(1-r)^{-\frac{5}{2}} \quad (41c)$$

As k' has a physical meaning of disruption density, so it should have real roots with $\alpha_1^2 + \frac{4\alpha_2 q_0}{1-r}$ being positive. And since $1-r > 0$, therefore, $\frac{d^2ATS}{dr^2}$ is always positive and indicates the fragility property of transportation systems when faced with supply disruption at the link level. Likewise to the proof of demand disruption, the Daganzo FD is a special case of the MoC, so we directly prove the fragility at the network level with MoC illustrated in the following section. \square

Proposition 5. *Road transportation systems are fragile with the onset of supply disruptions at the network level.*

Proof. As the proof of fragility under supply disruption with cubic polynomial MFDs involves solving the roots for cubic equations, for simplicity reasons, we prove only with Daganzo MoC. Since the traffic demand q_0 is constant, the traffic density of the new stable state $k'(r)$ would be:

$$q_0 = (1-r)(u_i k'(r) + c_i) \quad (42a)$$

$$k'(r) = \frac{\frac{q_0}{1-r} - c_i}{u_i} \quad (42b)$$

And the ATS and its derivatives are:

$$ATS = \frac{lk'(r)}{q_0} = \frac{l}{q_0 u_i} \left(\frac{q_0}{1-r} - c_i \right) \quad (43a)$$

$$\frac{dATS}{dr} = \frac{l}{u_i} (1-r)^{-2} \quad (43b)$$

$$\frac{d^2ATS}{dr^2} = \frac{2l}{u_i} (1-r)^{-3} \quad (43c)$$

As per Assumption 2, when studying supply disruptions, we focus on the uncongested zone of the MFD, meaning the slope of these relevant cuts is positive so that both derivatives are positive. \square

Proposition 6. *Road transportation systems are fragile when going through the recovery process from supply disruptions.*

Proof. To study the possible fragile properties of road transportation networks regarding the recovery process from supply disruptions, we need to combine the conclusions from Proposition 3 and Proposition 5. In Proposition 3, we've proven the recovery process to be fragile when the

traffic state shifts from a more congested cut to a less congested cut on the Daganzo MFD, or to be neither fragile nor antifragile when it stays only on one single cut. Therefore, it can be mathematically summarized as $\frac{d^2TTS}{dn'^2} \geq 0$. Following Assumption 2, $a_i > 0$ holds as the cut is below the critical density, we can easily prove the first derivative $\frac{dTTS}{dn'}$ to be non-negative as well with Eq. 23a, Eq. 26a, and Eq. 30a through the same procedure as proving the second derivative to be positive. And for the proof of recovery from supply disruptions, as shown in Fig. 8, likewise to Proposition 5, the relationship between the original and new equilibrium points before and after MFD disruptions can be expressed as:

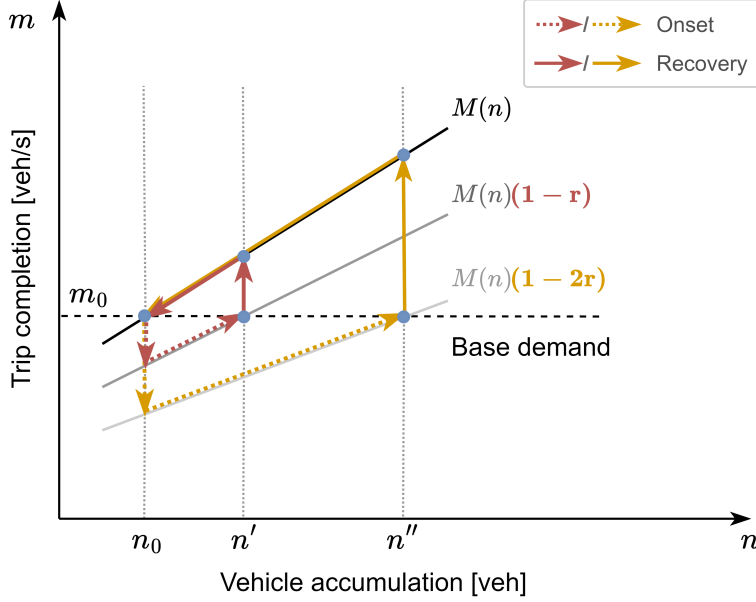


Figure 8: Recovery from supply disruption

$$m_0 = u_i n_0 + c_i = (1-r)(u_i n' + c_i) \quad (44a)$$

$$\implies n'(r) = \frac{u_i n_0 + c_i}{u_i(1-r)} - c_i/u_i \quad (44b)$$

The first and second derivatives of n' over the supply disruption magnitude coefficient r are:

$$\frac{dn'}{dr} = \frac{u_i n_0 + c_i}{u_i} (1-r)^{-2} \quad (45a)$$

$$\frac{d^2n'}{dr^2} = \frac{2(u_i n_0 + c_i)}{u_i} (1-r)^{-3} \quad (45b)$$

Since u_i and $u_i n_0 + c_i$ are both positive, the derivatives of n' over r are positive as well. Additionally, it can be easily proven that when considering the transition from a less congested to a more congested cut, the same conclusion also holds. As TTS is a function of n' and n' is again a function of r , by applying the chain rule, we can get the second derivative of TTS over r as:

$$\begin{aligned}
\frac{d^2TTS}{dr^2} &= \frac{d}{dr} \left(\frac{dTTS}{dn'} \cdot \frac{dn'}{dr} \right) \\
&= \frac{d^2TTS}{dn'^2} \cdot \left(\frac{dn'}{dr} \right)^2 + \frac{dTTS}{dn'} \cdot \frac{d^2n'}{dr^2}
\end{aligned} \tag{46}$$

Because all the four components of the Eq. 46 have been demonstrated above to be non-negative, thus $\frac{d^2TTS}{dn'^2}$ is also non-negative and we've proven the fragile nature of road transportation systems regarding the recovery process of supply disruptions. □

5. Fragility indicator and implications

Although road transportation systems have been mathematically proven to be intrinsically fragile, a quantitative approach to assess fragility across various networks is yet absent. It can also be of great interest to reveal factors contributing to or mitigating the fragile property of a road network. In Section 3, two generic methods, namely, second derivative and skewness for evaluating fragility have been discussed. Despite being proven to be positive and thus showcasing fragile, the exact value of the second derivatives varies even for different traffic states on the same MFD, let alone a cross-comparison among MFDs of various networks. Therefore, we resort to a skewness-based fragility indicator, so that one fixed value can be generated for a region based on the performance loss density distribution from multiple disruption recovery processes. For a given network, without considering hysteresis and other sources of uncertainties, a well-defined MFD can be produced and is widely utilized in the research of traffic control (Yildirimoglu and Geroliminis, 2014). Assuming no alteration in the driving behavior of the population, the well-defined MFD is primarily considered to be solely dependent on the network topology, including traffic control and signalization (Leclercq and Geroliminis, 2013). Therefore, in this section, we propose to develop a skewness-based indicator to evaluate the fragility of a given network, using only the MFD-related parameters obtained through analytical methods. This approach avoids the need for traffic sensor data, such as those from loop detectors, allowing for a pre-assessment of the network fragility early on during the design phase.

5.1. Empirical study on the skewness

As there is no direct way to define such a skewness-based indicator, we first design a unit MFD and empirically study the relationship between the skewness and the MFD-related parameters. Although typically more than three cuts can be generated to form an MFD through MoC, researchers sometimes simplify MFDs to be a trapezoidal shape with one forward, one stationary, and one backward cut (Tilg et al., 2020; Lee et al., 2023), which is sometimes also adopted for traffic control (Haddad and Geroliminis, 2012). In this section, we follow this simplification to facilitate creating a so-called unit MFD, similar to the isosceles FD proposed in Laval (2023), for the evaluation of fragility, formulated as $m = M(n, a_f, a_w, m_{\max}, n_{\max})$, where a_f and a_w each denotes the forward cut and the backward cut, or a_N and a_1 respectively. In addition, m_{\max} represents the maximal trip completion derived from the stationary cut. As maximal vehicle accumulation, denoted as n_{\max} , is another indispensable parameter in MoC, for the proposed unit MFD, we fix n_{\max} at 10000 veh, resembling the n_{\max} generated for the city center of Zurich in Fig. 12(b). An MFD for any given network can be scaled up or down to match the n_{\max} of the

unit MFD for cross-comparison. The real skewness of the network, denoted as s , is calculated as the asymmetry of the probability density distribution of TTS from multiple recovery processes with the same MFD but under different disruption magnitudes. With μ and σ denoting the mean and standard deviation, the skewness can be formulated as:

$$s = \frac{1}{N_{sample}} \sum_{i=1}^{N_{sample}} \left(\frac{TTS_i - \mu}{\sigma} \right)^3 \quad (47)$$

To ensure fair comparison, certain criteria have to be met. First, it is assumed that there is no base demand in the network. Second, when calculating TTS, the initial disruption vehicle accumulation n' follows a uniform distribution ranging between 5% and 95% of the maximal accumulation n_{max} . The interval for vehicle increment for this setting is 50, so a total number of 180 data points are sampled. It is worth highlighting that to calculate skewness, a sufficient number of samples is required to reach satisfactory accuracy, and the chosen number of samples is substantially above the minimal threshold based on some pre-experiments. Also note these conditions merely serve as a reference instead of strict requirements, meaning that a range between 10% and 90% may also be used for determining the skewness. However, a larger range renders the skewness of different networks more distinguishable. Once the experiment setup is established, the aim is then to approximate the estimated skewness of a given network, denoted as \tilde{s} , based on its MFD-related parameters and a proposed approximation function $\tilde{s} = f(a_f, a_w, m_{max})$.

One assumption for the analysis is $|a_w| \leq a_f$. As per [Daganzo \(1994\)](#), the backward wave travels several times slower than the free flow speed so the FD is formulated with a wave speed $|w| \leq u_f$. We also adopt the same assumption for the fragility indicator, although some further elaboration is needed. The FD is built on the analog with the hydrodynamic theory, where the well-known phenomenon of water hammer often occurs, which is a detrimental pressure surge when abruptly forcing to stop fluid motion in a rigid pipe ([Ghidaoui et al., 2005](#)). The pressure wave can propagate at a subsonic speed through the liquid along the pipe, which is considerably faster than the water flow speed, showing the possibility of backward wave speed being higher than the free flow speed. The major difference between traffic flow and water flow is the existence of safety distance in the former, but little gap in the latter. It can be easily proven that if the safety distance during driving could be the same as the effective vehicle length, the backward wave speed would equal the free flow speed. Therefore, it needs to be acknowledged that with the advancements in vehicular technologies such as Connected AVs (CAVs), which can form long platoons with minimal distance buffers, there is a likelihood that the backward wave speed could exceed the free flow speed in the future.

In [Fig. 9](#), we present the heatmaps of s as a function of $|a_w|$ and a_f for different values of m_{max} . Since the maximal vehicle accumulation $n_{max} = 10000$, which means a gradient $a_f \leq \cdot 10^{-4}$ will lead to the critical vehicle accumulation $n_c \geq n_{max}$, and therefore, both axes representing a_f and $|a_w|$ begin from $1.2 \cdot 10^{-4}$ instead of 10^{-4} or even 0. The contour lines are also illustrated to indicate multiple levels of skewness. Several patterns can be observed based on the contour lines, which represent an implicit function between skewness and the MFD-related parameters $|a_w| = f(a_f, m_{max}, s)$ instead of $s = f(a_f, a_w, m_{max})$:

Observation 1. For the contour lines with the same skewness across different values of m_{max} , it can be found that m_{max} has a scaling effect, which can be mathematically formulated as [Eq. 48](#). For example, in [Fig. 9\(e\)](#) with $m_{max} = 1.5$, the contour line with $s = 1.3$ crosses approximately

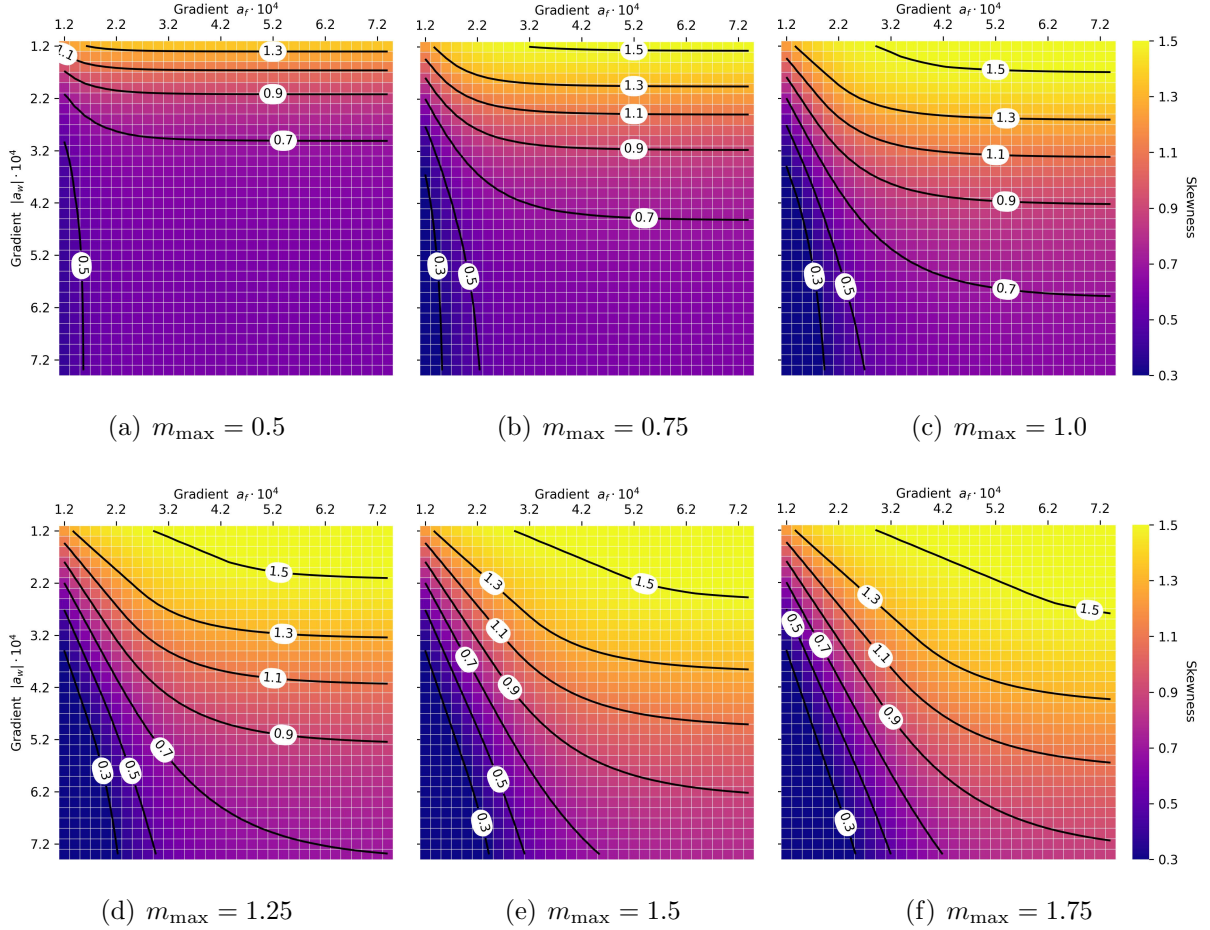


Figure 9: Skewness s heatmap with a_f and a_w across different m_{\max}

the point $(a_f, |a_w|) = (6.2, 3.8)$, which means in Fig. 9(b) with $m_{\max} = 0.75$, half of the m_{\max} in Fig. 9(e), the same contour line $s = 1.3$ will cross the point $(a_f, |a_w|) = (3.1, 1.9)$. This observation will be further discussed and validated later.

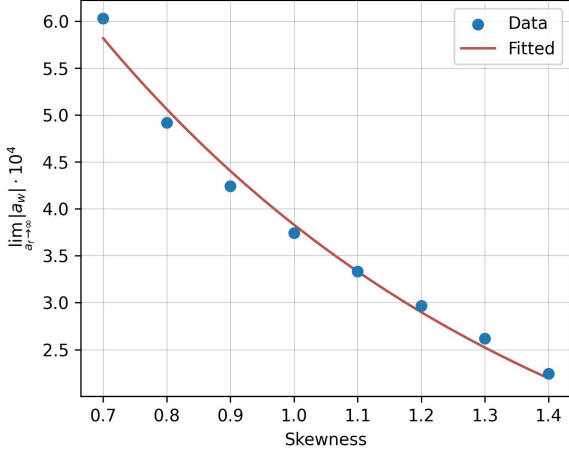
$$\frac{|a_w|}{m_{\max}} = f\left(\frac{a_f}{m_{\max}}, \tilde{s}\right) \quad (48)$$

Observation 2. According to the assumption that $|a_w| \leq a_f$, we mainly focus on the upper triangular matrix. And for each skewness contour line within the upper triangular matrix, $|a_w|$ becomes a constant value when a_f increases to infinity. However, it should be acknowledged that the contour lines with very low skewness in the lower triangular matrix do not specifically follow this observation. An exponential relationship can be roughly approximated between $|a_w|$ and skewness \tilde{s} with coefficients β_1 , β_2 , and β_3 , as shown in Fig. 10(a), which can be mathematically formulated as:

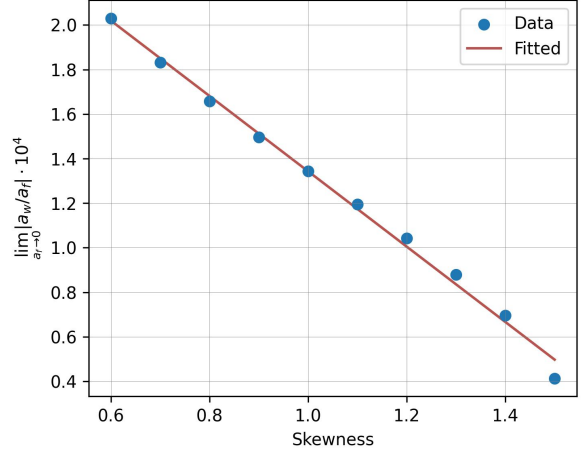
$$\lim_{a_f \rightarrow \infty} |a_w| = \beta_1 e^{\beta_2(\tilde{s} - \beta_3)} \quad (49)$$

Observation 3. For each skewness contour line, when a_f gets closer to 0, the initial gradient of the contour line $\lim_{a_f \rightarrow 0} \left| \frac{a_w}{a_f} \right|$ will also become a constant. And when extended towards the upper left, they intercept exactly at the origin of the coordinates $(a_f, |a_w|) = (0, 0)$. The relationship between the gradient of the contour line $\lim_{a_f \rightarrow 0} \left| \frac{a_w}{a_f} \right|$ and skewness \tilde{s} can be roughly approximated as a linear function, as shown in Fig. 10(b), which can be mathematically formulated as:

$$\lim_{a_f \rightarrow 0} \left| \frac{a_w}{a_f} \right| = \beta_4 \tilde{s} + \beta_5 \quad (50)$$



(a) Approximation of $\lim_{a_f \rightarrow \infty} |a_w|$



(b) Approximation of $\lim_{a_f \rightarrow 0} \left| \frac{a_w}{a_f} \right|$

Figure 10: Approximation of the coefficients

5.2. Skewness-based fragility indicator

The above observations suggest a significant relationship between the skewness and the MFD-related parameters worth further exploitation. Based on Observations 2 and Observation 3, these contour lines have been found to share great similarities with certain types of functions in the family of sigmoid curves. In this work, we call such approximators as activation functions $y = f_{\text{activation}}(x)$, with the term borrowed from the deep learning domain, where the hyperbolic tangent $f_{\text{tanh}}(x) = \frac{e^x - e^{-x}}{e^x + e^{-x}}$ is one of the most commonly applied functional forms. Likewise to Observation 2, the hyperbolic tangent function has a constant value at the right end $\lim_{x \rightarrow \infty} f_{\text{tanh}}(x) = 1$. And for Observation 3, a similar property can be observed that the gradient of the activation function at origin is also a constant $f'_{\text{tanh}}(0) = 1$.

To scale the activation function to a certain skewness contour line according to these two observations to generate our proposed approximation function $f_{\text{approx}}(\cdot)$, the below two conditions are to be satisfied:

$$\lim_{a_f \rightarrow \infty} f_{\text{approx}}(a_f) = \lim_{a_f \rightarrow \infty} |a_w| \cdot \lim_{a_f \rightarrow \infty} f_{\text{tanh}}(a_f) \quad (51a)$$

$$\lim_{a_f \rightarrow 0} \frac{f_{\text{approx}}(a_f)}{a_f} = \lim_{a_f \rightarrow 0} \left| \frac{a_w}{a_f} \right| \cdot \lim_{a_f \rightarrow 0} \frac{f_{\text{tanh}}(a_f)}{a_f} \quad (51b)$$

Therefore, the activation function for the approximation of skewness s needs to be rewritten as:

$$\begin{aligned} a_w &= f_{\text{approx}}(a_f) \\ &= \lim_{a_f \rightarrow \infty} |a_w| \cdot f_{\text{tanh}} \left(\frac{\lim_{a_f \rightarrow 0} \left| \frac{a_w}{a_f} \right|}{\lim_{a_f \rightarrow \infty} |a_w|} \cdot a_f \right) \end{aligned} \quad (52)$$

Now taking Observation 1 into account as well, and with coefficients $\beta_{1,\dots,5}$ being able to be approximated with Eq. 49, Eq. 50, and Fig. 10, the proposed approximation function is:

$$\frac{a_w}{m_{\text{max}}} = \beta_1 e^{\beta_2(\tilde{s}-\beta_3)} \cdot f_{\text{tanh}} \left(\frac{\beta_4 \tilde{s} + \beta_5}{\beta_1 e^{\beta_2(\tilde{s}-\beta_3)}} \cdot \frac{a_f}{m_{\text{max}}} \right) \quad (53)$$

Despite being an implicit function, the skewness \tilde{s} can be solved with an iterative optimization algorithm, such as the Powell hybrid method or its modifications. Although with both ends $a_f \rightarrow 0$ and $a_f \rightarrow \infty$ of the contour lines being fixed, the hyperbolic tangent function alone does not necessarily guarantee a rather decent approximation. Hence, we introduce some other activation functions that resemble the hyperbolic tangent function with a list below, which will be applied and cross-compared for the approximation of the skewness of a network. All these activation functions share the same characteristics that $\lim_{x \rightarrow \infty} f_{\text{activation}}(x) = 1$ and $f'_{\text{activation}}(0) = 1$, but with varying curvature to reach $a_f \rightarrow \infty$:

- Error function: $f_{\text{erf}}(x) = \frac{2}{\sqrt{\pi}} \int_0^x e^{-t^2} dt$
- Gudermannian function: $f_{\text{gd}}(x) = 2 \arctan(\tanh(\frac{x}{2}))$
- Arctangent function: $f_{\text{arctan}}(x) = \frac{2}{\pi} \arctan(\frac{2}{\pi}x)$
- Inverted square root unit: $f_{\text{isru}}(x) = \frac{x}{\sqrt{1+x^2}}$
- A generalized form of the inverted square root unit: $f_{\kappa}(x) = \frac{x}{(1+|x|^{\kappa})^{1/\kappa}}$

5.3. Validation

To validate the effectiveness of our proposed skewness-based fragility indicator, the approximation error Δs between the real skewness s from the unit MFD and the approximated skewness \tilde{s} of each activation function is computed and presented in Fig. 11 with $m_{\text{max}} = 1$. In Fig. 11(a) we select $k = 5$ to represent the generalized form of the inverted square root unit. A darker shade of red or blue indicates the skewness from the approximation \tilde{s} is greater or smaller than the real value s . It can be observed that the activation functions $f_{\kappa=5}$ and f_{erf} show seemingly superior performance, with the vast majority of the heatmap cells lying below a $|\Delta s|$ of 0.1. It should also be noted that at the upper margin of the heatmap with $a_f \gg |a_w|$, particularly for $f_{\kappa=5}$ and f_{erf} , a red strip with significant positive error can be observed. We acknowledge but accept the rather large error in the red strip, for the same reason as the lower triangular matrix $a_f < |a_w|$, this strip with $a_f \gg |a_w|$ lacks realism either.

To better quantify the error Δs from different approximation functions, we summarize the error into Table 3 with Mean Absolute Error (MAE), Mean Squared Error (MSE), and Root Mean

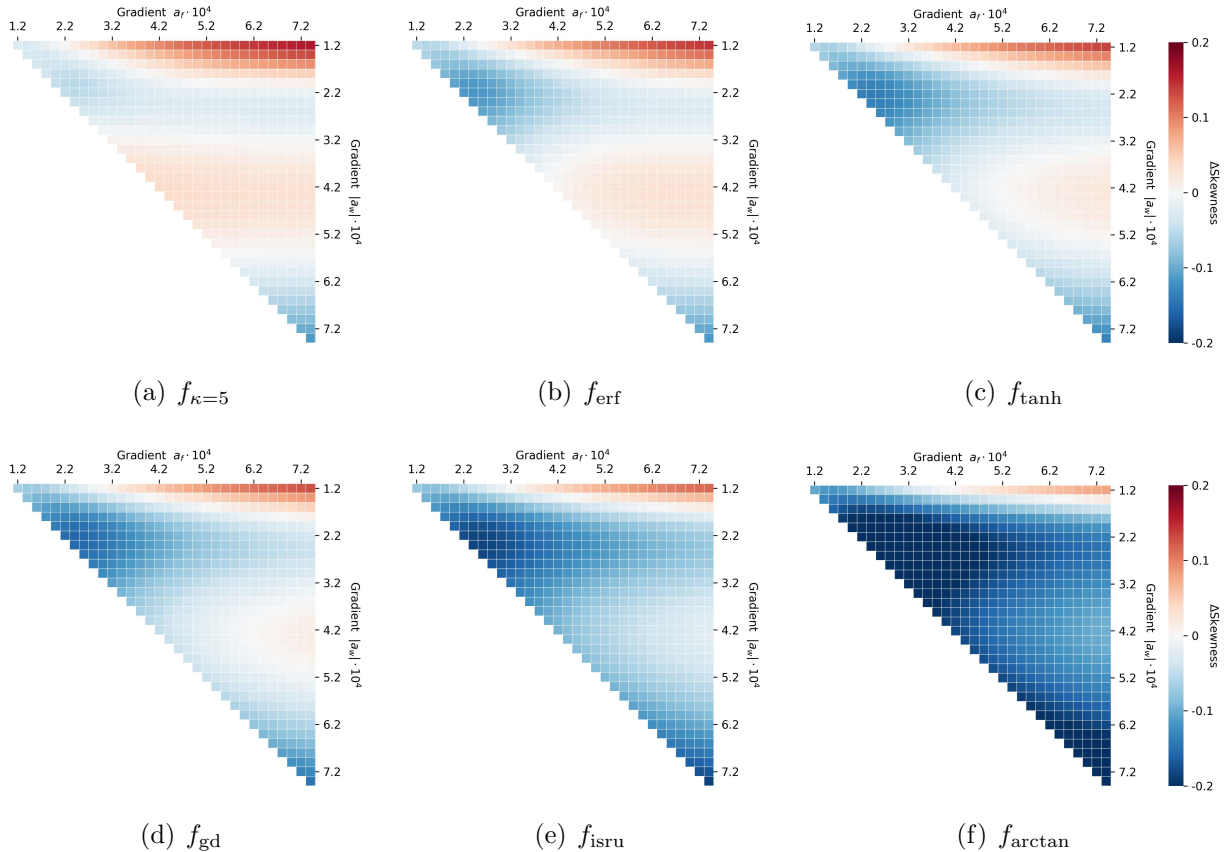


Figure 11: Error of approximation by applying different activation functions with $m_{\max} = 1$

Square Error (RMSE). Other values of κ for the generalized form of the inverted square root unit f_{κ} are also presented. The activation function $f_{\kappa=5}$ showcased the best performance, with an MAE and an RMSE being 0.032 and 0.043 respectively. Considering the skewness in the upper triangular matrix in Fig. 9(c) varies roughly between 0.7 – 1.5 and shows an average skewness of 1.136, the MAE and RMSE demonstrate an error well below 5% and thus validate the accuracy of our proposed approximation function. With $f_{\kappa=5}$, we also showcase the approximation accuracy for varying values of m_{\max} in Table 3. While the error still lies below 5% with m_{\max} larger than 1, the accuracy deteriorates when m_{\max} becomes smaller. This is partially attributable to the function form of approximation in Eq. 49 and Eq. 50 as well as the coefficients $\beta_{1,\dots,5}$. The current coefficients are approximated with the data points from a trimmed range in Fig. 10 to achieve the least error in the case of $m_{\max} = 1$. If a slightly larger range is considered, a rather uniform value of RMSE at around 0.75 – 0.85 can be observed regardless of the different values of m_{\max} , roughly 7% of the average skewness, validating the Observation 1. Also, for the approximation of $\lim_{a_f \rightarrow \infty} |a_w|$, a polynomial can be applied in replacement of the current exponential function to achieve potential better performance.

5.4. Implications

Aside from the proposed approximation function to estimate the skewness-based fragility indicator, insights into the fragility together with the MFD-related parameters can also be drawn from the heatmaps in Fig. 9. When $|a_w|$ is not sufficiently large, an increase in a_f contributes to the network’s fragility, whereas a larger $|a_w|$ reduces such fragility. The implications are twofold:

Table 3: Error of approximation of applying different activation functions

Function	MAE	MSE	RMSE	With $f_{\kappa=5}$	MAE	MSE	RMSE
f_{erf}	0.037	0.0023	0.048	$m_{\text{max}} = 0.5$	0.120	0.034	0.185
f_{tanh}	0.044	0.0033	0.057	$m_{\text{max}} = 0.75$	0.044	0.0045	0.067
f_{gd}	0.054	0.0045	0.067	$m_{\text{max}} = 1.0$	0.032	0.0018	0.043
f_{isru}	0.084	0.0089	0.094	$m_{\text{max}} = 1.25$	0.034	0.0023	0.048
f_{arctan}	0.152	0.0261	0.162	$m_{\text{max}} = 1.5$	0.038	0.0026	0.051
$f_{\kappa=4}$	0.033	0.0019	0.043	$m_{\text{max}} = 1.75$	0.040	0.0028	0.053
$f_{\kappa=5}$	0.032	0.0018	0.043				
$f_{\kappa=6}$	0.032	0.0019	0.044				

- To minimize urban traffic accident rates and reduce noise pollution, aligned with the long-term goal of Vision Zero in the EU and worldwide to reach no traffic fatalities and severe injuries (Doecke et al., 2020), many cities have implemented stricter speed limits, such as the Tempo 30 regulation in Zurich (Menendez and Ambühl, 2022). Although this may reduce the overall serviceability of the urban road networks, it enhances the city’s antifragility when dealing with traffic disruptions.
- While backward wave speed is generally linked to the driving behavior of human-driven vehicles, Makridis et al. (2024) recently found that adaptive cruise control, a precursor to AVs, can increase backward wave speed with minimum headway settings (although still not as fast as free-flow speed), suggesting that introducing AVs into transportation systems could potentially improve the network’s antifragility. However, this enhancement of antifragility at the macroscopic level may result in fragility at the microscopic level, as minimum safety distances can cause propagating string instability under perturbations (Makridis et al., 2021), if the connectivity and cooperation levels are not sufficiently high.

6. Numerical simulation

Even though researchers generally consider MFDs to be well-defined, road transportation systems in the real world and their MFDs are always subject to stochasticity all the time, as shown in Geroliminis and Daganzo (2008); Ambühl et al. (2021), and this is the same case for FDs as well (Siqueira et al., 2016; Qu et al., 2017). Therefore, when validating a newly proposed traffic control algorithm, it has become a common practice to account for model uncertainties and showcase the method’s robustness, such as in Geroliminis et al. (2013); Haddad and Mirkin (2017); Zhou and Gayah (2023). In our study, however, the model stochasticity cannot be directly reflected in the mathematical analysis, hence, it is indispensable to show the influence of realistic stochasticity on the fragile nature of transportation systems with a numerical simulation, i.e., whether the system still maintains the same fragile response under real-world errors in MFD when a demand or supply disruption is present.

6.1. Experimental setup with real-world parameters

In this section, we simulate the disruption recovery process. The MFD of the studied region is generated by applying MoC following [Daganzo and Geroliminis \(2008\)](#) with realistic parameters in the city center of Zurich. Some parameters, e.g., free-flow speed, back-propagation speed, maximal density, and capacity are provided in [Ambühl et al. \(2020\)](#) for Zurich with queried routes in Google API and with other validation methods. The total and average lane length for the city center is determined through SUMO with OpenStreetMap API. The average trip length of Zurich is studied in [Schüssler and Axhausen \(2008\)](#). We introduce stochasticity in the city center of Zurich with real traffic light data, which is publicized by the Statistical Office of Zurich and accessible in [Genser et al. \(2023, 2024\)](#). The authors acknowledge that MoC is developed with the premise of a homogeneous region, and given that the available data is limited to only one main intersection in this region, we assume that this intersection serves as a representative sample for the city center region. Also, since the signalization in Zurich is actuated based on the present traffic flow, they do not strictly follow a fixed-time signal cycle. Despite this actuation, a concentrated distribution can be easily observed in the dataset and we assume the green split of the cycle follows a normal distribution. The offset is presumed zero as the assumption for the actuated signal in Yokohama in [Daganzo and Geroliminis \(2008\)](#). According to the daily average traffic density of Zurich in [Ambühl et al. \(2021\)](#), we approximate the traffic demand, which is also the trip completion when the traffic state is at equilibrium, is about 0.6 veh/s for our studied region. This corresponds to an accumulation of around 975 vehicles in the city center. The parameters and the related values are summarized in Table 4.

Table 4: Real-world parameters for the city center of Zurich

Parameters	Notation	Unit	Value
Free-flow speed	u_l	m/s	12.5
Backward wave speed	w_l	m/s	6.0
Maximal density	k_{\max}	veh/m	0.145
Capacity	c_l	veh/s	0.51
Total lane length	D	m	68631
Average lane length	l	m	167
Average trip length	L	m	7110
Signal cycle time	C	s	50
Signal green time (mean)	μ_G	s	14.8
Signal green time (std.)	σ_G	s	2.5
Offset	δ	s	0
Traffic demand	m_0	veh/s	0.6

The average green time of the signal is 14.8 s and its standard deviation is 2.5 s. With an interval of one standard deviation, i.e., a set of green time $\mathcal{G} = \{\mu_G - \sigma_G, \mu_G, \mu_G + \sigma_G\}$, and following the MoC described in [Daganzo and Geroliminis \(2008\)](#), we can produce stationary, forward, and backward cuts in gray, blue, and red lines, for each of the MFD with a unique green time from \mathcal{G} , as Fig. 12(a) shows with dotted lines, solid lines, and dashed lines. The MFD with a longer green time $\mu_G + \sigma_G$ yields a greater MFD and vice versa. The MFDs share the same maximal vehicle density of around 0.145 veh/m, which corresponds to a gridlock accumulation of about 10000 vehicles for the studied region based on Eq. 2a and Eq. 2b. In the following

simulations for demand and supply disruptions with realistic model stochasticity, we study the congestion dissipation processes in the road network as traffic recovers from disruptions. At each timestep, a stochastic signal green time is sampled following normal distribution $G \sim \mathcal{N}(14.8, 2.5)$ based on real-world data, leading to an uncertain MFD profile as Fig. 12(b) shows. The green scattering points connected with thin dotted lines display an example of a congestion dissipation process with an initial disruption of about 7000 vehicles and are sampled from every 100th point for clarity.

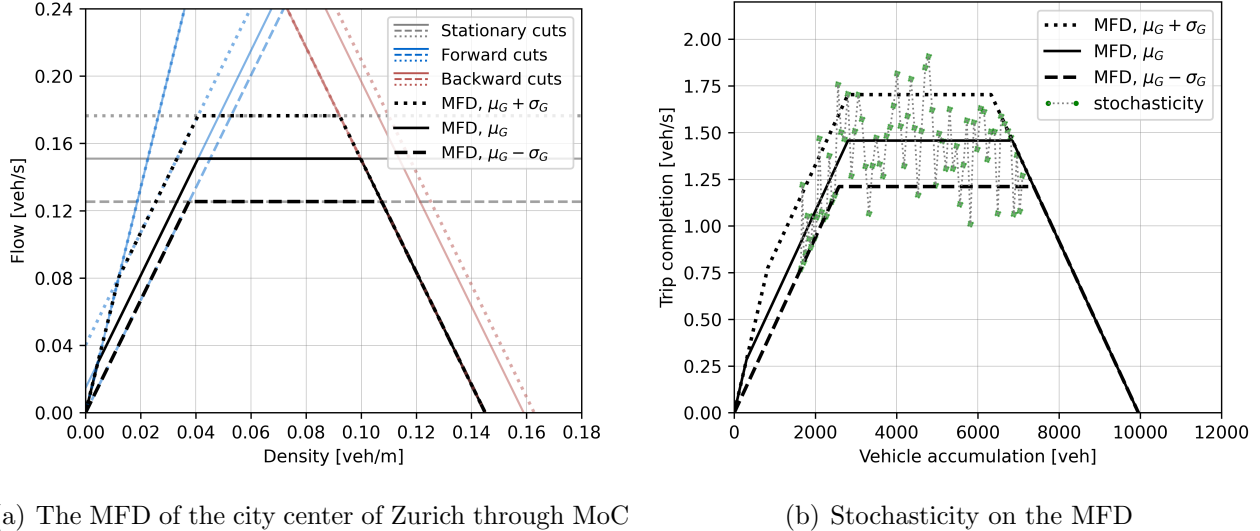
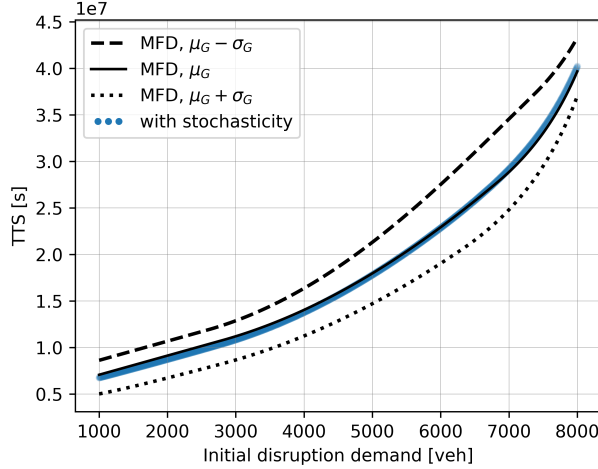


Figure 12: The MFD of the city center of Zurich through MoC and stochasticity

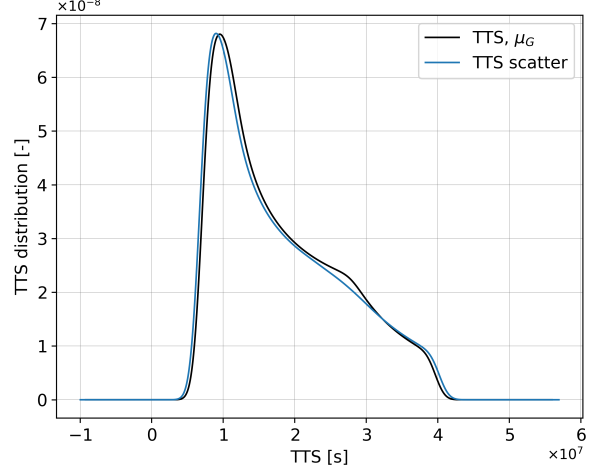
6.2. Demand disruptions

Now we start the numerical simulation with different initial disruption demands n' from 1000 to 8000 vehicles. The simulation time is 7200 seconds for each scenario with different initial demands. Fig. 13(a) demonstrates that TTS grows exponentially with linearly increasing initial disruption demand, which validates the fragile nature proved with mathematical analysis. The solid, dashed, or dotted line each represents the TTS calculated under the three deterministic MFDs with green time in \mathcal{G} . Other than the black curves, there are also 1000 scattering points forming the blue curve. Each scatter point is composed of a full disruption recovery process sampled following uniform distribution $n' \sim U(1000, 8000)$.

Since the blue curve composed from the scattering points closely aligns with the solid curve, it can be inferred that the influence of realistic stochasticity on the MFD is mostly negligible. Nevertheless, an intriguing observation is that, when the disruption demand is relatively low, the blue curve dips slightly below the MFD of the solid curve. However, the blue curve appears to exceed the TTS of the well-defined MFD when the demand is substantial. This may indicate that the recovery process with stochasticity can possibly have a larger second derivative (although two linear curves share the same second derivative of zero but different slopes can yield a similar observation). When we show the distribution of these two curves, as in Fig. 13(b), the TTS with stochasticity has a more concentrated distribution at a lower value while having a marginally longer tail pointing to the right, showing a more left-skewed distribution compared to the one without realistic stochasticity. This can also be validated by calculating the skewness of these



(a) Demand disruption and TTS



(b) TTS distribution w/o stochasticity

Figure 13: Numerical simulation for demand disruption with stochasticity

two curves. When there is no stochasticity, the skewness is 0.67 while the skewness for the blue curve has a value of 0.70. As a greater skewness indicates a more fragile system, it means by introducing realistic stochasticity, the urban road network becomes even more fragile. It makes particular sense that as per definition, a fragile system should exhibit a much more degraded performance with larger disruptions brought by stochasticity, resulting in poor adaptability to uncertainties.

6.3. Supply disruptions

Likewise, we showcase that supply disruptions can strengthen the fragile nature of transportation systems as well. With the same simulation environment, instead of the linearly increasing initial disruption demand, now a linearly growing supply disruption magnitude coefficient r from 0 to 0.5 is considered. The simulation of the recovery process from the supply disruption along with 1000 uniformed sampled points $r \sim U(0, 0.5)$ is shown in Fig. 14(a). First of all, as the blue curve with stochasticity lies below the curve from the deterministic MFD with the mean green time, it means that the network with stochasticity has a better performance. This performance improvement can be attributed to the fact that, prior to reaching the maximal capacity, the upper MFD in the dotted curve generated from MoC keeps a larger space from the solid curve MFD profile compared to the distance between the lower MFD in the dashed curve. Therefore, although the likelihood of sampling a trip completion above or below the mean MFD profile is the same, there is a higher probability that the gained value of trip completion will surpass the loss caused by stochasticity. Despite this gain in system performance, when we calculate the skewness of distribution, we get a value of 0.49 for the deterministic MFD and 0.53 for the MFD with uncertainty, demonstrating again that stochasticity escalates the fragile response of the road transportation systems. Hence, the transportation systems have been demonstrated to be fragile with numerical simulation and such fragility has been reinforced with stochasticity in this work.

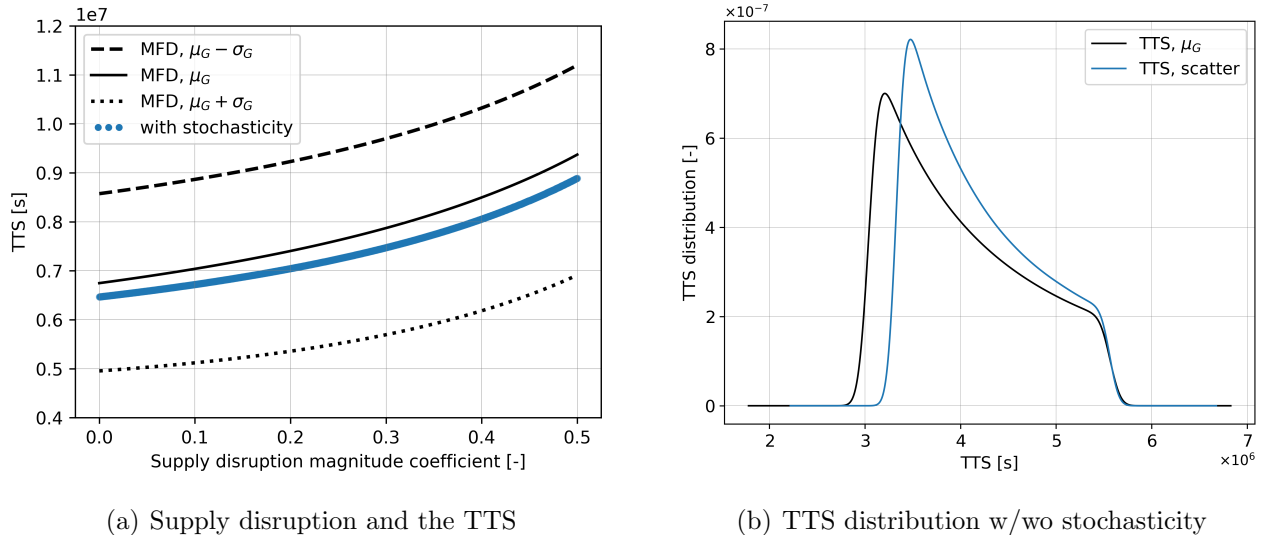


Figure 14: Numerical simulation for supply disruption with stochasticity

7. Conclusion

This research introduces the pioneering concept of (anti-)fragility and its detection under the context of transportation. Then it systematically demonstrates the fragile nature of road transportation systems through rigorous mathematical analysis. With established traffic models, namely FDs and MFDs, as the representation of the system dynamics, the second derivative of the system performance loss over the magnitudes of disruptions can be proven to be positive, indicating the fragile property. To achieve a universal conclusion, the fragility of the road transportation systems is validated from multiple perspectives: at the link level or the network level; under disruption from the demand or the supply side; and for the onset of disruption or the recovery from disruption. With such fragile nature established, this research also proposes a generic approach for quantifying and assessing network fragility by using a scalable unit MFD and a skewness-based indicator. An approximation function inspired by the Sigmoid curve has been developed for accurately determining the skewness, enabling the approximation and cross-comparison of the fragility of different networks using merely MFD-related parameters at hand. The proposed fragility indicator can be potentially applied to evaluate the fragility of future new infrastructures and transportation policies. Additionally, through a numerical simulation with realistic data, including topology attributes, driving behavior, signalization, etc., results suggest that real-world stochasticity has a limited effect on the fragile characteristics of road transportation systems but contributes to rendering the system even more fragile.

Several limitations of this study need to be acknowledged. Although uncertainties are explicitly accounted for in the numerical simulation, this research largely relies on the assumptions of homogenous networks and well-defined MFDs as in many other research works (Haddad and Mirkin, 2017; Zhou and Gayah, 2021; Genser and Kouvelas, 2022). Since hysteresis is a commonly observed phenomenon due to unevenly distributed traffic congestion, it can be of great interest to involve heterogeneity and hysteresis in future studies of antifragility. As hysteresis leads to a decrease in network serviceability, it can potentially be regarded as a virtual supply disruption. Additionally in Section 5, it is assumed that the backward wave is slower than the free flow speed, allowing for a relatively accurate skewness estimation with the proposed

approximation function, but as noted, this assumption may be challenged by technological advancements, particularly with the rise of CAVs, highlighting the necessity for developing more precise approximation functions to address future challenges.

This study aims to offer insights to researchers, emphasizing the fragile nature of road transportation systems. Potential extensions of this work can be multifold. For instance, this study lays a theoretical foundation and complements our ongoing work on data-driven antifragile traffic control, countering the intrinsic fragility of road networks through induced antifragility. Furthermore, as early findings have pointed out the possibilities of applying MFDs in other transportation modes, the fragility demonstrated in urban road networks may well be extended to various transportation systems or even systems in other disciplines with similar characteristics. Given that network performance assessment in modern times should not rely on a sole criterion based on efficiency, a multi-objective framework should be developed in the future, incorporating factors such as efficiency, antifragility, sustainability, safety, and more.

8. CRediT authorship contribution statement

Linghang Sun: Conceptualization, Investigation, Methodology, Visualization, Writing – original draft. Yifan Zhang: Methodology, Visualization, Writing - review & editing. Cristian Axenie: Project administration, Resources, Writing - review & editing. Margherita Grossi: Project administration, Resources, Writing - review & editing. Anastasios Kouvelas: Supervision, Writing - review & editing. Michail A. Makridis: Conceptualization, Methodology, Supervision, Writing - review & editing.

9. Declaration of Competing Interest

This research was kindly funded by the Huawei Munich Research Center under the framework of the Antigones project, with one of our co-authors being employed at the said company. Otherwise, the authors declare that they have no known competing financial interests or personal relationships that could have appeared to influence the work reported in this paper.

References

- Ambühl, L., Loder, A., Bliemer, M.C., Menendez, M., Axhausen, K.W., 2020. A functional form with a physical meaning for the macroscopic fundamental diagram. *Transportation Research Part B: Methodological* 137, 119–132. doi:[10.1016/j.trb.2018.10.013](https://doi.org/10.1016/j.trb.2018.10.013).
- Ambühl, L., Loder, A., Leclercq, L., Menendez, M., 2021. Disentangling the city traffic rhythms: A longitudinal analysis of MFD patterns over a year. *Transportation Research Part C: Emerging Technologies* 126, 103065. doi:[10.1016/j.trc.2021.103065](https://doi.org/10.1016/j.trc.2021.103065).
- Ambühl, L., Loder, A., Zheng, N., Axhausen, K.W., Menendez, M., 2019. Approximative Network Partitioning for MFDs from Stationary Sensor Data. *Transportation Research Record* 2673, 94–103. doi:[10.1177/0361198119843264](https://doi.org/10.1177/0361198119843264).
- Ampountolas, K., Zheng, N., Geroliminis, N., 2017. Macroscopic modelling and robust control of bi-modal multi-region urban road networks. *Transportation Research Part B: Methodological* 104, 616–637. doi:[10.1016/j.trb.2017.05.007](https://doi.org/10.1016/j.trb.2017.05.007).

- Axenie, C., Kurz, D., Saveriano, M., 2022. Antifragile Control Systems: The Case of an Anti-Symmetric Network Model of the Tumor-Immune-Drug Interactions. *Symmetry* 14, 2034. doi:[10.3390/sym14102034](https://doi.org/10.3390/sym14102034).
- Axenie, C., López-Corona, O., Makridis, M.A., Akbarzadeh, M., Saveriano, M., Stancu, A., West, J., 2024. Antifragility in complex dynamical systems. *npj Complexity* 1, 1–8. doi:[10.1038/s44260-024-00014-y](https://doi.org/10.1038/s44260-024-00014-y).
- Axenie, C., Saveriano, M., 2023. Antifragile Control Systems: The Case of Mobile Robot Trajectory Tracking Under Uncertainty and Volatility. *IEEE Access* 11, 138188–138200. doi:[10.1109/ACCESS.2023.3339988](https://doi.org/10.1109/ACCESS.2023.3339988).
- Büchel, B., Marra, A.D., Corman, F., 2022. COVID-19 as a window of opportunity for cycling: Evidence from the first wave. *Transport Policy* 116, 144–156. doi:[10.1016/j.tranpol.2021.12.003](https://doi.org/10.1016/j.tranpol.2021.12.003).
- Calvert, S.C., Snelder, M., 2018. A methodology for road traffic resilience analysis and review of related concepts. *Transportmetrica A: Transport Science* 14, 130–154. doi:[10.1080/23249935.2017.1363315](https://doi.org/10.1080/23249935.2017.1363315).
- Cats, O., 2016. The robustness value of public transport development plans. *Journal of Transport Geography* 51, 236–246. doi:[10.1016/j.jtrangeo.2016.01.011](https://doi.org/10.1016/j.jtrangeo.2016.01.011).
- Chen, C., Huang, Y.P., Lam, W.H.K., Pan, T.L., Hsu, S.C., Sumalee, A., Zhong, R.X., 2022. Data efficient reinforcement learning and adaptive optimal perimeter control of network traffic dynamics. *Transportation Research Part C: Emerging Technologies* 142, 103759. doi:[10.1016/j.trc.2022.103759](https://doi.org/10.1016/j.trc.2022.103759).
- Coppitters, D., Contino, F., 2023. Optimizing upside variability and antifragility in renewable energy system design. *Scientific Reports* 13, 9138. doi:[10.1038/s41598-023-36379-8](https://doi.org/10.1038/s41598-023-36379-8).
- Corman, F., D’Ariano, A., Hansen, I.A., 2014. Evaluating Disturbance Robustness of Railway Schedules. *Journal of Intelligent Transportation Systems* 18, 106–120. doi:[10.1080/15472450.2013.801714](https://doi.org/10.1080/15472450.2013.801714).
- Corman, F., Henken, J., Keyvan-Ekbatani, M., 2019. Macroscopic fundamental diagrams for train operations - are we there yet?, in: *2019 6th International Conference on Models and Technologies for Intelligent Transportation Systems (MT-ITS)*, pp. 1–8. doi:[10.1109/MTITS.2019.8883374](https://doi.org/10.1109/MTITS.2019.8883374).
- Corman, F., Quaglietta, E., Goverde, R.M.P., 2018. Automated real-time railway traffic control: an experimental analysis of reliability, resilience and robustness. *Transportation Planning and Technology* 41, 421–447. doi:[10.1080/03081060.2018.1453916](https://doi.org/10.1080/03081060.2018.1453916).
- Daganzo, C.F., 1994. The cell transmission model: A dynamic representation of highway traffic consistent with the hydrodynamic theory. *Transportation Research Part B: Methodological* 28, 269–287. doi:[10.1016/0191-2615\(94\)90002-7](https://doi.org/10.1016/0191-2615(94)90002-7).
- Daganzo, C.F., 2005. A variational formulation of kinematic waves: basic theory and complex boundary conditions. *Transportation Research Part B: Methodological* 39, 187–196. doi:[10.1016/j.trb.2004.04.003](https://doi.org/10.1016/j.trb.2004.04.003).

- Daganzo, C.F., Geroliminis, N., 2008. An analytical approximation for the macroscopic fundamental diagram of urban traffic. *Transportation Research Part B: Methodological* 42, 771–781. doi:[10.1016/j.trb.2008.06.008](https://doi.org/10.1016/j.trb.2008.06.008).
- Daganzo, C.F., Lehe, L.J., Argote-Cabanero, J., 2018. Adaptive offsets for signalized streets. *Transportation Research Part B: Methodological* 117, 926–934. doi:[10.1016/j.trb.2017.08.011](https://doi.org/10.1016/j.trb.2017.08.011).
- Dickerson, A., Peirson, J., Vickerman, R., 2000. Road Accidents and Traffic Flows: An Economic Investigation. *Economica* 67, 101–121. doi:[10.1111/1468-0335.00198](https://doi.org/10.1111/1468-0335.00198).
- Doecke, S.D., Baldock, M.R.J., Kloeden, C.N., Dutschke, J.K., 2020. Impact speed and the risk of serious injury in vehicle crashes. *Accident Analysis & Prevention* 144, 105629. doi:[10.1016/j.aap.2020.105629](https://doi.org/10.1016/j.aap.2020.105629).
- Federal Statistical Office of Switzerland, 2020. *Mobilität und Verkehr: Panorama - 2020 | Publikation*.
- Genser, A., Kouvelas, A., 2022. Dynamic optimal congestion pricing in multi-region urban networks by application of a Multi-Layer-Neural network. *Transportation Research Part C: Emerging Technologies* 134, 103485. doi:[10.1016/j.trc.2021.103485](https://doi.org/10.1016/j.trc.2021.103485).
- Genser, A., Makridis, M.A., Yang, K., Abmühl, L., Menendez, M., Kouvelas, A., 2023. A traffic signal and loop detector dataset of an urban intersection regulated by a fully actuated signal control system. *Data in Brief* 48, 109117. doi:[10.1016/j.dib.2023.109117](https://doi.org/10.1016/j.dib.2023.109117).
- Genser, A., Makridis, M.A., Yang, K., Ambühl, L., Menendez, M., Kouvelas, A., 2024. Time-to-Green Predictions for Fully-Actuated Signal Control Systems With Supervised Learning. *IEEE Transactions on Intelligent Transportation Systems* , 1–14doi:[10.1109/TITS.2023.3348634](https://doi.org/10.1109/TITS.2023.3348634).
- Geroliminis, N., Daganzo, C.F., 2008. Existence of urban-scale macroscopic fundamental diagrams: Some experimental findings. *Transportation Research Part B: Methodological* 42, 759–770. doi:[10.1016/j.trb.2008.02.002](https://doi.org/10.1016/j.trb.2008.02.002).
- Geroliminis, N., Haddad, J., Ramezani, M., 2013. Optimal Perimeter Control for Two Urban Regions With Macroscopic Fundamental Diagrams: A Model Predictive Approach. *IEEE Transactions on Intelligent Transportation Systems* 14, 348–359. doi:[10.1109/TITS.2012.2216877](https://doi.org/10.1109/TITS.2012.2216877).
- Ghidaoui, M.S., Zhao, M., McInnis, D.A., Axworthy, D.H., 2005. A Review of Water Hammer Theory and Practice. *Applied Mechanics Reviews* 58, 49–76. doi:[10.1115/1.1828050](https://doi.org/10.1115/1.1828050).
- Greenshields, B.D., Thompson, J.T., Dickinson, H.C., Swinton, R.S., 1934. The photographic method of studying traffic behavior. *Highway Research Board Proceedings* 13.
- Haddad, J., Geroliminis, N., 2012. On the stability of traffic perimeter control in two-region urban cities. *Transportation Research Part B: Methodological* 46, 1159–1176. doi:[10.1016/j.trb.2012.04.004](https://doi.org/10.1016/j.trb.2012.04.004).
- Haddad, J., Mirkin, B., 2017. Coordinated distributed adaptive perimeter control for large-scale urban road networks. *Transportation Research Part C: Emerging Technologies* 77, 495–515. doi:[10.1016/j.trc.2016.12.002](https://doi.org/10.1016/j.trc.2016.12.002).

- Haddad, J., Shraiber, A., 2014. Robust perimeter control design for an urban region. *Transportation Research Part B: Methodological* 68, 315–332. doi:[10.1016/j.trb.2014.06.010](https://doi.org/10.1016/j.trb.2014.06.010).
- Isaacson, D., Robinson, J., Swenson, H., Denery, D., 2010. A Concept for Robust, High Density Terminal Air Traffic Operations, in: 10th AIAA Aviation Technology, Integration, and Operations (ATIO) Conference. American Institute of Aeronautics and Astronautics. doi:[10.2514/6.2010-9292](https://doi.org/10.2514/6.2010-9292).
- Kim, H., Muñoz, S., Osuna, P., Gershenson, C., 2020. Antifragility Predicts the Robustness and Evolvability of Biological Networks through Multi-Class Classification with a Convolutional Neural Network. *Entropy* 22, 986. doi:[10.3390/e22090986](https://doi.org/10.3390/e22090986).
- Laval, J.A., 2023. Self-organized criticality of traffic flow: Implications for congestion management technologies. *Transportation Research Part C: Emerging Technologies* 149, 104056. doi:[10.1016/j.trc.2023.104056](https://doi.org/10.1016/j.trc.2023.104056).
- Laval, J.A., Castrillón, F., 2015. Stochastic approximations for the macroscopic fundamental diagram of urban networks. *Transportation Research Part B: Methodological* 81, 904–916. doi:[10.1016/j.trb.2015.09.002](https://doi.org/10.1016/j.trb.2015.09.002).
- Leclercq, L., Geroliminis, N., 2013. Estimating MFDs in simple networks with route choice. *Transportation Research Part B: Methodological* 57, 468–484. doi:[10.1016/j.trb.2013.05.005](https://doi.org/10.1016/j.trb.2013.05.005).
- Leclercq, L., Ladino, A., Becarie, C., 2021. Enforcing optimal routing through dynamic avoidance maps. *Transportation Research Part B: Methodological* 149, 118–137. doi:[10.1016/j.trb.2021.05.002](https://doi.org/10.1016/j.trb.2021.05.002).
- Lee, G., Ding, Z., Laval, J., 2023. Effects of loop detector position on the macroscopic fundamental diagram. *Transportation Research Part C: Emerging Technologies* 154, 104239. doi:[10.1016/j.trc.2023.104239](https://doi.org/10.1016/j.trc.2023.104239).
- Lo, H.K., Luo, X.W., Siu, B.W.Y., 2006. Degradable transport network: Travel time budget of travelers with heterogeneous risk aversion. *Transportation Research Part B: Methodological* 40, 792–806. doi:[10.1016/j.trb.2005.10.003](https://doi.org/10.1016/j.trb.2005.10.003).
- Makridis, M., Mattas, K., Anesiadou, A., Ciuffo, B., 2021. OpenACC. An open database of car-following experiments to study the properties of commercial ACC systems. *Transportation Research Part C: Emerging Technologies* 125, 103047. doi:[10.1016/j.trc.2021.103047](https://doi.org/10.1016/j.trc.2021.103047).
- Makridis, M.A., Kouvelas, A., Laval, J.A., 2024. Platoon Fundamental Diagram estimation can be Markovian: evidence from human- and self-driven vehicle trajectories. doi:[10.48550/arXiv.2401.17065](https://doi.org/10.48550/arXiv.2401.17065).
- Mariotte, G., Leclercq, L., Laval, J.A., 2017. Macroscopic urban dynamics: Analytical and numerical comparisons of existing models. *Transportation Research Part B: Methodological* 101, 245–267. doi:[10.1016/j.trb.2017.04.002](https://doi.org/10.1016/j.trb.2017.04.002).
- Marra, A.D., Sun, L., Corman, F., 2022. The impact of COVID-19 pandemic on public transport usage and route choice: Evidences from a long-term tracking study in urban area. *Transport Policy* 116, 258–268. doi:[10.1016/j.tranpol.2021.12.009](https://doi.org/10.1016/j.tranpol.2021.12.009).

- Matthias, V., Bieser, J., Mocanu, T., Pregger, T., Quante, M., Ramacher, M.O.P., Seum, S., Winkler, C., 2020. Modelling road transport emissions in Germany – Current day situation and scenarios for 2040. *Transportation Research Part D: Transport and Environment* 87, 102536. doi:[10.1016/j.trd.2020.102536](https://doi.org/10.1016/j.trd.2020.102536).
- Mattsson, L.G., Jenelius, E., 2015. Vulnerability and resilience of transport systems – A discussion of recent research. *Transportation Research Part A: Policy and Practice* 81, 16–34. doi:[10.1016/j.tra.2015.06.002](https://doi.org/10.1016/j.tra.2015.06.002).
- Menendez, M., Ambühl, L., 2022. Implementing Design and Operational Measures for Sustainable Mobility: Lessons from Zurich. *Sustainability* 14, 625. doi:[10.3390/su14020625](https://doi.org/10.3390/su14020625).
- Nahmias-Biran, B.h., Oke, J.B., Kumar, N., 2021. Who benefits from AVs? Equity implications of automated vehicles policies in full-scale prototype cities. *Transportation Research Part A: Policy and Practice* 154, 92–107. doi:[10.1016/j.tra.2021.09.013](https://doi.org/10.1016/j.tra.2021.09.013).
- Ng, M., Waller, S.T., 2010. A computationally efficient methodology to characterize travel time reliability using the fast Fourier transform. *Transportation Research Part B: Methodological* 44, 1202–1219. doi:[10.1016/j.trb.2010.02.008](https://doi.org/10.1016/j.trb.2010.02.008).
- Qu, X., Zhang, J., Wang, S., 2017. On the stochastic fundamental diagram for freeway traffic: Model development, analytical properties, validation, and extensive applications. *Transportation Research Part B: Methodological* 104, 256–271. doi:[10.1016/j.trb.2017.07.003](https://doi.org/10.1016/j.trb.2017.07.003).
- Rodrigues, F., Azevedo, C.L., 2019. Towards Robust Deep Reinforcement Learning for Traffic Signal Control: Demand Surges, Incidents and Sensor Failures, in: *2019 IEEE Intelligent Transportation Systems Conference (ITSC)*, pp. 3559–3566. doi:[10.1109/ITSC.2019.8917451](https://doi.org/10.1109/ITSC.2019.8917451).
- Ruel, J.J., Ayres, M.P., Ruel, J.J., Ayres, M.P., 1999. Jensen’s inequality predicts effects of environmental variation. *Trends in Ecology & Evolution* 14, 361–366. doi:[10.1016/S0169-5347\(99\)01664-X](https://doi.org/10.1016/S0169-5347(99)01664-X).
- Saedi, R., Saeedmanesh, M., Zockaie, A., Saberi, M., Geroliminis, N., Mahmassani, H.S., 2020. Estimating network travel time reliability with network partitioning. *Transportation Research Part C: Emerging Technologies* 112, 46–61. doi:[10.1016/j.trc.2020.01.013](https://doi.org/10.1016/j.trc.2020.01.013).
- Safadi, Y., Fu, R., Quan, Q., Haddad, J., 2023. Macroscopic Fundamental Diagrams for Low-Altitude Air city Transport. *Transportation Research Part C: Emerging Technologies* 152, 104141. doi:[10.1016/j.trc.2023.104141](https://doi.org/10.1016/j.trc.2023.104141).
- Saidi, S., Koutsopoulos, H.N., Wilson, N.H.M., Zhao, J., 2023. Train following model for urban rail transit performance analysis. *Transportation Research Part C: Emerging Technologies* 148, 104037. doi:[10.1016/j.trc.2023.104037](https://doi.org/10.1016/j.trc.2023.104037).
- Schüssler, N., Axhausen, K.W., 2008. Identifying trips and activities and their characteristics from gps raw data without further information. *Arbeitsberichte Verkehrs-und Raumplanung* 502.
- Shang, W.L., Gao, Z., Daina, N., Zhang, H., Long, Y., Guo, Z., Ochieng, W.Y., 2022. Benchmark Analysis for Robustness of Multi-Scale Urban Road Networks Under Global Disruptions. *IEEE Transactions on Intelligent Transportation Systems* , 1–11doi:[10.1109/TITS.2022.3149969](https://doi.org/10.1109/TITS.2022.3149969).

- Siqueira, A.F., Peixoto, C.J.T., Wu, C., Qian, W.L., 2016. Effect of stochastic transition in the fundamental diagram of traffic flow. *Transportation Research Part B: Methodological* 87, 1–13. doi:[10.1016/j.trb.2016.02.003](https://doi.org/10.1016/j.trb.2016.02.003).
- Sirmatel, I.I., Geroliminis, N., 2018. Economic Model Predictive Control of Large-Scale Urban Road Networks via Perimeter Control and Regional Route Guidance. *IEEE Transactions on Intelligent Transportation Systems* 19, 1112–1121. doi:[10.1109/TITS.2017.2716541](https://doi.org/10.1109/TITS.2017.2716541).
- Sun, L., Makridis, M.A., Genser, A., Axenie, C., Grossi, M., Kouvelas, A., 2024. Antifragile Perimeter Control: Anticipating and Gaining from Disruptions with Reinforcement Learning.
- Taleb, N.N., 2012. *Antifragile: Things That Gain from Disorder*. Reprint edition ed., Random House Publishing Group, New York.
- Taleb, N.N., Douady, R., 2013. Mathematical definition, mapping, and detection of (anti)fragility. *Quantitative Finance* 13, 1677–1689. doi:[10.1080/14697688.2013.800219](https://doi.org/10.1080/14697688.2013.800219).
- Tang, J., Heinemann, H., Han, K., Luo, H., Zhong, B., 2020. Evaluating resilience in urban transportation systems for sustainability: A systems-based Bayesian network model. *Transportation Research Part C: Emerging Technologies* 121, 102840. doi:[10.1016/j.trc.2020.102840](https://doi.org/10.1016/j.trc.2020.102840).
- Tilg, G., Ambühl, L., Batista, S.F.A., Menéndez, M., Leclercq, L., Busch, F., 2023. From Corridor to Network Macroscopic Fundamental Diagrams: A Semi-Analytical Approximation Approach. *Transportation Science* 57, 1115–1133. doi:[10.1287/trsc.2022.0402](https://doi.org/10.1287/trsc.2022.0402).
- Tilg, G., Amini, S., Busch, F., 2020. Evaluation of analytical approximation methods for the macroscopic fundamental diagram. *Transportation Research Part C: Emerging Technologies* 114, 1–19. doi:[10.1016/j.trc.2020.02.003](https://doi.org/10.1016/j.trc.2020.02.003).
- U.S. Bureau of Public Roads, 1964. *Traffic assignment manual for application with a large, high speed computer*. US Department of Commerce.
- U.S. Congress, Office of Technology Assessment, 1984. *Airport system development*. U.S. Government Printing Office.
- U.S. Department of Transportation, 2019. *Vehicle Miles Traveled*.
- Wang, J.Y.T., Ehrgott, M., Chen, A., 2014. A bi-objective user equilibrium model of travel time reliability in a road network. *Transportation Research Part B: Methodological* 66, 4–15. doi:[10.1016/j.trb.2013.10.007](https://doi.org/10.1016/j.trb.2013.10.007).
- Yang, K., Menendez, M., Zheng, N., 2019. Heterogeneity aware urban traffic control in a connected vehicle environment: A joint framework for congestion pricing and perimeter control. *Transportation Research Part C: Emerging Technologies* 105, 439–455. doi:[10.1016/j.trc.2019.06.007](https://doi.org/10.1016/j.trc.2019.06.007).
- Yildirimoglu, M., Geroliminis, N., 2014. Approximating dynamic equilibrium conditions with macroscopic fundamental diagrams. *Transportation Research Part B: Methodological* 70, 186–200. doi:[10.1016/j.trb.2014.09.002](https://doi.org/10.1016/j.trb.2014.09.002).

- Zhang, R., Zhang, J., 2021. Long-term pathways to deep decarbonization of the transport sector in the post-COVID world. *Transport Policy* 110, 28–36. doi:[10.1016/j.tranpol.2021.05.018](https://doi.org/10.1016/j.tranpol.2021.05.018).
- Zhou, D., Gayah, V.V., 2021. Model-free perimeter metering control for two-region urban networks using deep reinforcement learning. *Transportation Research Part C: Emerging Technologies* 124, 102949. doi:[10.1016/j.trc.2020.102949](https://doi.org/10.1016/j.trc.2020.102949).
- Zhou, D., Gayah, V.V., 2023. Scalable multi-region perimeter metering control for urban networks: A multi-agent deep reinforcement learning approach. *Transportation Research Part C: Emerging Technologies* 148, 104033. doi:[10.1016/j.trc.2023.104033](https://doi.org/10.1016/j.trc.2023.104033).
- Zhou, Y., Wang, J., Yang, H., 2019. Resilience of Transportation Systems: Concepts and Comprehensive Review. *IEEE Transactions on Intelligent Transportation Systems* 20, 4262–4276. doi:[10.1109/TITS.2018.2883766](https://doi.org/10.1109/TITS.2018.2883766).